3-2020

An Assessment of the Spatial Variation of Isotopic Ratios in a CANDU-6 Reactor for Nuclear Treaty Monitoring

Aaron W. Burkhardt

AN ASSESSMENT OF THE SPATIAL VARIATION OF ISOTOPIC RATIOS IN A CANDU-6 REACTOR FOR NUCLEAR TREATY MONITORING

THESIS

Aaron W. Burkhardt, Second Lieutenant, USAF

AFIT-ENP-MS-20-M-086

DEPARTMENT OF THE AIR FORCE
AIR UNIVERSITY

AIR FORCE INSTITUTE OF TECHNOLOGY

Wright-Patterson Air Force Base, Ohio

AFIT-ENP-MS-20-M-086

AN ASSESSMENT OF THE SPATIAL VARIATION OF ISOTOPIC RATIOS IN A CANDU-6 REACTOR FOR NUCLEAR TREATY MONITORING

THESIS

Presented to the Faculty

Department of Engineering Physics

Graduate School of Engineering and Management

Air Force Institute of Technology

Air University

Air Education and Training Command

in Partial Fulfillment of the Requirements for the

Degree of Master of Science

Aaron W. Burkhardt, BS

Second Lieutenant, USAF

March 2020

AFIT-ENP-MS-20-M-086

AN ASSESSMENT OF THE SPATIAL VARIATION OF ISOTOPIC RATIOS IN A CANDU-6 REACTOR FOR NUCLEAR TREATY MONITORING

THESIS

Aaron W. Burkhardt, BS
Second Lieutenant, USAF

Committee Membership:

Maj James E. Bevins, Ph.D.
Chair

Dr. Abigail A. Bickley
Member

Dr. Robert M. Smith
Member

Abstract

The Preparatory Commission for the Comprehensive Nuclear Test Ban Treaty Organization developed the International Monitoring System for monitoring nuclear explosive testing and compliance with nuclear treaties. Many of the International Monitoring System stations are capable of detecting radionuclides that can be used to determine their origin and creation environment. However, there is not a single unique signature associated with each creation environment. Nuclear reactors, for example, can have a wide range of isotopic concentrations caused by spatial variations in neutron flux intensity and energy. As a single sample only provides a single isotopic ratio measurement, this can make disambiguation difficult for systems that have varying, and potentially overlapping, signatures. To better quantify this phenomenon, a 3-D quarter-core CANDU-6 was modeled using Serpent 2 to analyze the spatial flux distribution and develop a spent fuel isotopic concentration database. The model showed an overall relative total flux spatial difference of $45.1 \pm 4.5\%$ and significant spatial differences in discrete neutron energies ranging from 1 to 30%. The developed database provides the full spatial isotopic concentration distribution for 257 isotopes expected from CANDU-6 spent fuel. Actinide and fission product isotopic ratios were analyzed to determine their range and associated confidence intervals. The ratios showed significant bundle-to-bundle variance and significant inter-isotope distribution variance making it difficult to accurately assess the range of possibilities from analytic methods. The developed CANDU-6 spatial isotopic concentration database provides increased resolution for future analysis of International Monitoring System signatures thereby enhancing the capabilities of the system to effectively perform their treaty monitoring mission.

Acknowledgements

I would like to thank and acknowledge Maj Bevins and Dr. Bickley for their knowledge and aid in guiding me in this work, and Dr. Holland and Dr. Leppänen for their computational expertise and assistance in the operation of the models and codes.

Aaron W. Burkhardt

Table of Contents

Page

List of Figures

List of Tables

AN ASSESSMENT OF THE SPATIAL VARIATION OF ISOTOPIC RATIOS IN A CANDU-6 REACTOR FOR NUCLEAR TREATY MONITORING

I. Introduction

The Comprehensive Nuclear-Test-Ban Treaty Organization (CTBTO) maintains the International Monitoring System (IMS) to detect proliferant activities [1,2]. This system consists of a network of 337 locations utilizing sensors for seismic, hydroacoustic, infrasound, and radionuclide detection. The raw data from the radionuclide sensors are compared to databases of known, characteristic isotopic ratio signatures to determine their origin. Therefore, the effectiveness of these sensors is dictated by the sensitivity of the equipment used and the accuracy of the databases measurements are compared to. The accuracy of these databases comes into question for "edge cases" where the signature is not clearly a treaty-violating activity nor treaty-allowed activity [3,4]. While there is a large set of of experimental data, empirical evaluations, and approximated models, the full range of possible signatures for a given activity is rarely fully quantified.

Nuclear reactors experience spatial variation in the neutron flux intensity and energy spectrum thereby resulting in spatial changes in isotopic concentrations. Macro evidence of this is the fuel shuffling performed by Pressurized Water Reactors (PWRs) and Boiling Water Reactors (BWRs) to maintain criticality [5]. Fuel bundles located at different regions of the reactor experience different neutron flux profiles and inherently different burnup profiles. This variation creates a range of characteristic

isotopic ratio signatures from a given nuclear reactor, which makes identifying single representative ratios an impossibility. The development of a full database based on the spatial variation within a reactor would provide a baseline for future evaluations and more accurate adjudication of edge case signatures.

1.1 Background

Reactor modeling is not a new subject of exploration to the nuclear community. Models are built for every aspect of a reactor – from simple criticality calculations to detailed operational performance and safety assurance [5]. These models can incorporate a variety of complex physics including 3D neutronics, fuel burnup calculations, computational fluid dynamics, and heat transfer; however, almost all are simplified to target a specific problem due to the computationally intensive nature of full-core, time-dependent reactor models.

Reactor burnup models are most often used to evaluate the performance of the fuel over an operational period [5]. This allows the visualization of macro-scale results used in reactor design. These models allow the testing of designs under different conditions to determine system behavior. As such, information including criticality, power production, and averaged isotopic ratios are sufficient in describing the system as a whole for accurate results.

The standard isotopic ratio signatures of nuclear reactors are often determined from generalized models that use a variety of approximations [3, 4]. These include limited or no axial variation, core-averaged isotopic concentrations, infinite systems, and linear isotope production. These approximations may be valid for calculating averaged isotopic concentrations, but do not account for the spatial neutron flux spectrum and resulting isotopic concentration variation throughout a reactor that can be important for treaty monitoring applications.

Significant research has been performed for the purpose of determining fuel optimization for reactor operation and performance. A small subset of this research also exists for the purpose of identifying the probable sources of origin of environmental samples. Two examples of this research were performed by Martin Robel of Lawrence Livermore National Laboratory.

The first example examines discriminating source reactor type from uranium and plutonium concentrations in fuel of unknown pedigree [3]. Robel explored the use of multivariate statistical analysis to determine the reactor class most closely associated with a particular isotopic ratio. The reference data used was created by ORIGEN, the common "gold standard" for isotopic ratio analysis of reactors [6]. However, as Robel notes, the results are representative of the fuel assemblies as a whole and do not account for possible variation within a core.

The second example from Robel's research used position independent isotopic ratios of reactor fuel to determine their production history [4]. This research used experimental measurements of spent fuel and models to evaluate isotopic ratios that do not vary axially within a fuel assembly to obtain a first order analytical solution. Again, this work acknowledges the variability of isotopic ratios throughout a reactor, but focuses on a static assembly and ratios that presumably do not vary within said assembly.

1.2 Research Problem and Objectives

The radioisotope sampling and nuclear treaty monitoring techniques used by the CTBTO measure characteristic isotopic ratios far from their origin point in nuclear reactors, accelerators, or prohibited nuclear activity. The origin of the release is a rarely known *a priori* [1, 2]. While most signatures can be cleanly classified, "edge cases" require a more thorough characterization of the emitting source to enable

adjudication [3, 4]. One source of these "edge cases" is the spatial variation seen throughout the reactor from which the sample originated. To increase the confidence in these measurements for determining proliferant activity, the potential variation in isotopic ratios that can be seen from reactor operation is explored using a common proliferant reactor, the Canada Deuterium Uranium Reactor (CANDU-6).

To accomplish this, a generalized Quarter-Core CANDU-6 model, based on the Georgia Institute of Technology (GIT) half-core model, is developed using Serpent2 and simulated for 500 fuel channel refuelings [7]. The initial and final model after all refuelings are analyzed for spatial flux variation and differences due to refueling. A single fuel bundle is modeled, courtesy of Lt. Stephen Baxter, and analyzed for intra-bundle isotopic ratio variance from burnup. Finally, the spent fuel from the quarter-core model is analyzed to determine the overall spent fuel isotopic concentration variation and develop a baseline for CANDU-6 reactors.

1.3 Methodology

The quarter-core CANDU model was developed using Serpent 2 to utilize modern Monte Carlo and burnup techniques [8]. A quarter-core model is used rather than a half-core or full-core model to leverage the radial symmetry of the CANDU-6 design to improve computational performance. More discrete planes of symmetry, such as eighth-core or half-axial, could not be used due to differences in the radial direction and the refueling pattern implemented. A generic initial loading of eight different bundle burnups was used for the initial criticality model. While this model maintains criticality, there are steep spatial gradients not representative of steady-state operation from the coarse binning of the initial burnup.

To overcome the limitations of the starting burnup profile, the model underwent 500 fuel channel refuelings. This created a more realistic distribution of burnup

profiles throughout the core and created the isotopic concentration database for evaluation. Checks were performed at each stage of the model to ensure that the model met all operational requirements, including source convergence, criticality, isotope production, and the results converged to steady state operational characteristics.

The spent fuel from the final refueling of each fuel channel was used to develop a spent fuel spatial isotopic concentration database. This database consists of 257 isotopic concentrations from 760 unique fuel bundles. Analysis was performed to evaluate the spatial distributions of select isotopic concentrations and ratios.

1.4 Assumptions and Limitations

Modeling and simulation often provides an easy, fast, and cheap method of finding a solution compared to experimental measurements. However, it has an Achilles' heel as it is based on approximations and/or empirical data. In other words, "all models are wrong; some are useful." This popular phrase among computational engineers has been adopted as the motto of this research. While all efforts were made to make the quarter-core CANDU-6 model useful, it is worth highlighting several assumptions and limitations that persist.

The first limitation is the lack of information available for creating the model. The GIT model is used as the baseline, and supplementary material from several reactor descriptions and schematics is used to fill in the gaps. This results in a generalized CANDU-6 model not related to any particular CANDU-6 reactor. As each CANDU-6 reactor is unique with a unique refueling pattern, this does not completely bound the range of expected isotopic ratio distributions, but provides a reasonable starting estimate and methodology.

The model also starts depletion in a fully operational state by artificially depleting fresh fuel bundles which skips the initial startup process, distinct burnup of fresh fuel,

and use of soluble boron. This artificial injection of uncertainty is slowly removed from the model by the several hundred refuelings used prior to extracting isotopic concentration results from each bundle. As such, the final results are representative of steady state operation and may miss variations due to start-up.

Lastly, due to limited computational resources and time, a few aspects of the model suffer from increased uncertainty up to 15%. The quarter-core CANDU-6 model contains 1140 unique bundles. As such, bundles located on the periphery of the core experience a lower magnitude in flux. To ensure the completion of 500 channel refuelings, an optimized population of neutrons was used to balance uncertainty and computational time. This resulted in 4.6% overall flux uncertainty and up to 15% discrete energy uncertainty for axial and radial peripheral bundles. This level of uncertainty is considered acceptable to obtain good overall results as its effect is solely on uncommon neutron energies. Additional quantitative details are discussed in Section 3.1.4 and Section 4.1.

1.5 Research Contributions

This research contributes to the fields of non-proliferation and reactor modeling in several notable aspects:

- **CANDU-6 spent fuel isotopic concentration baseline:** A database containing 237 isotopic concentrations in 760 unique spent fuel bundles is developed. This database is meant to serve as a reference source containing possible spent fuel isotopic concentrations and corresponding probabilities for a CANDU-6 reactor.

- **Isotopic ratio distributions:** An analysis of the range of isotopic ratios relevant to nuclear treaty monitoring is performed. This highlights the wide range

of isotopic concentrations that can be observed from CANDU-6 operations and illustrates the limitations of current generalized methods.

- **Reactor modeling methodology:** A new method for modeling nuclear reactors to determine the full spread of isotopic ratios relevant to nuclear treaty monitoring is documented.

II. Theory

To develop a spent fuel isotopic concentration database for non-proliferation, understanding current non-proliferation policy, the nuclear fuel cycle, and the operation and modeling of nuclear reactors is required. First, aspects of the fuel cycle and non-proliferation relevant to reactor modeling are discussed. Then, concepts of nuclear reactors pertaining to design, function, and operation are discussed with an extended focus towards the CANDU-6 reactor. Finally, an explanation of the 3D Monte Carlo reactor modeling techniques used in this research is provided. This information provides the baseline knowledge required for understanding the research methodology in Chapter 3 and the discussion of results in Chapter 4.

2.1 The Comprehensive Nuclear-Test-Ban Treaty Organization

The Comprehensive Nuclear-Test-Ban Treaty was written in 1996 as a means to monitor a proposed treaty on the prohibition of future nuclear weapons tests [1, 2, 9]. The treaty has not yet gone into effect as only 36 of 44 required states have ratified it; however, progress has been made in anticipation of its mission. The Preparatory Commission for the Comprehensive Nuclear-Test-Ban Treaty Organization (CTBTO), established in 1997, has set the framework for the CTBTO to conduct its mission – monitoring of nuclear events around the world to verify that states are complying with their treaty obligations – 180 days after the treaty is ratified.

The CTBTO's primary monitoring capability is through the International Monitoring System (IMS) [1, 2]. The IMS consists of 337 facilities around the world dedicated to monitoring the environment for signs of proliferation. The vast majority of these facilities, 321, are monitoring stations that use various sensor technologies, including seismic, hydroacoustic, and infrasound to collect data. Eighty of these mon-

itoring stations serve as radionuclide detectors that take and measure air samples to identify characteristic radionuclide signatures. These signatures are sensitive to their creation environment and, ideally, differ for a fission weapon detonation and nuclear reactor. The last 16 facilities not yet mentioned are radionuclide laboratories used to test these samples. Figure 2.1 shows the locations of these monitoring systems around the world.

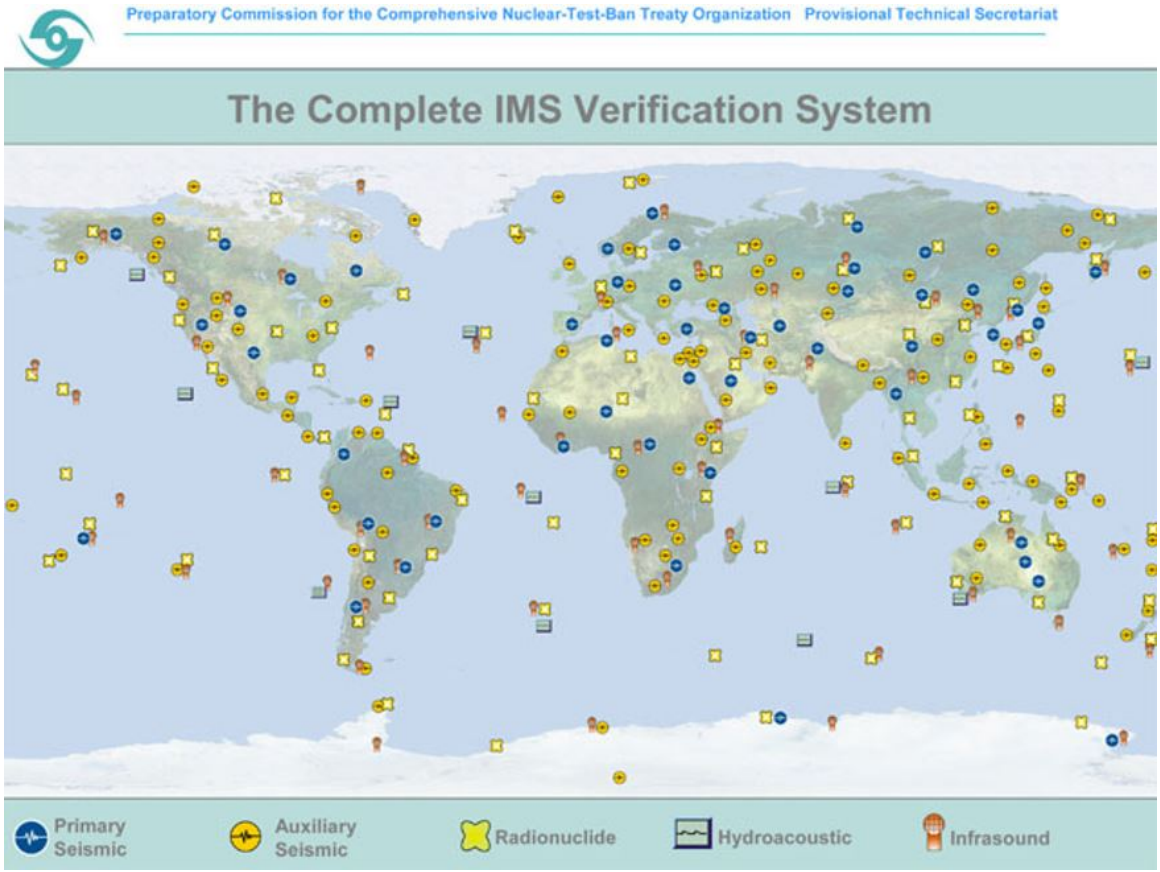

Figure 2.1. Locations of the 321 monitoring stations of the International Monitoring System [1, 2].

To determine whether a radionuclide sample could be indicative of a nuclear weapons test, it is compared to other samples of known proliferant and non-proliferant activities [1, 2, 9]. Figure 2.2 is an example of this comparison with xenon ratio measurements taken from several nuclear power plants (NPPs) and medical isotope production facilities (MIPFs). Points located to the left of the red line are indicative of

non-proliferant activities while points located to the right are indicative of *potential* proliferant activities. Because of the ambiguity of *potential* proliferant activity, it is important to understand the possible signatures a facility can produce based on standard operations to reduce potential false positives.

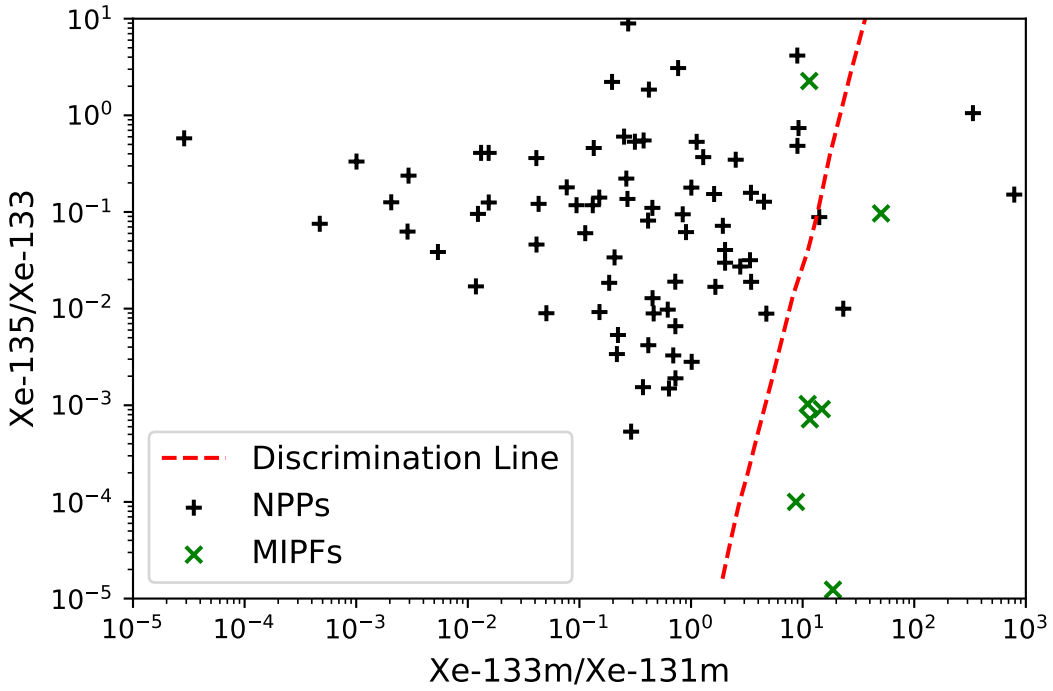

Figure 2.2. CTBTO xenon isotopic ratios from NPPs and MIPFs. The discrimination line is used to differentiate between non-proliferant and potentially proliferant activities [9].

2.2 The Nuclear Fuel Cycle

The nuclear fuel cycle is the open, or closed in the case of fuel reprocessing, loop that describe the path of uranium from mining to power production [10]. It consists of several steps shown in Figure 2.3 including the procurement of base materials, manufacturing of fuel, use in reactors, and disposal; all vital to the operation of NPPs.

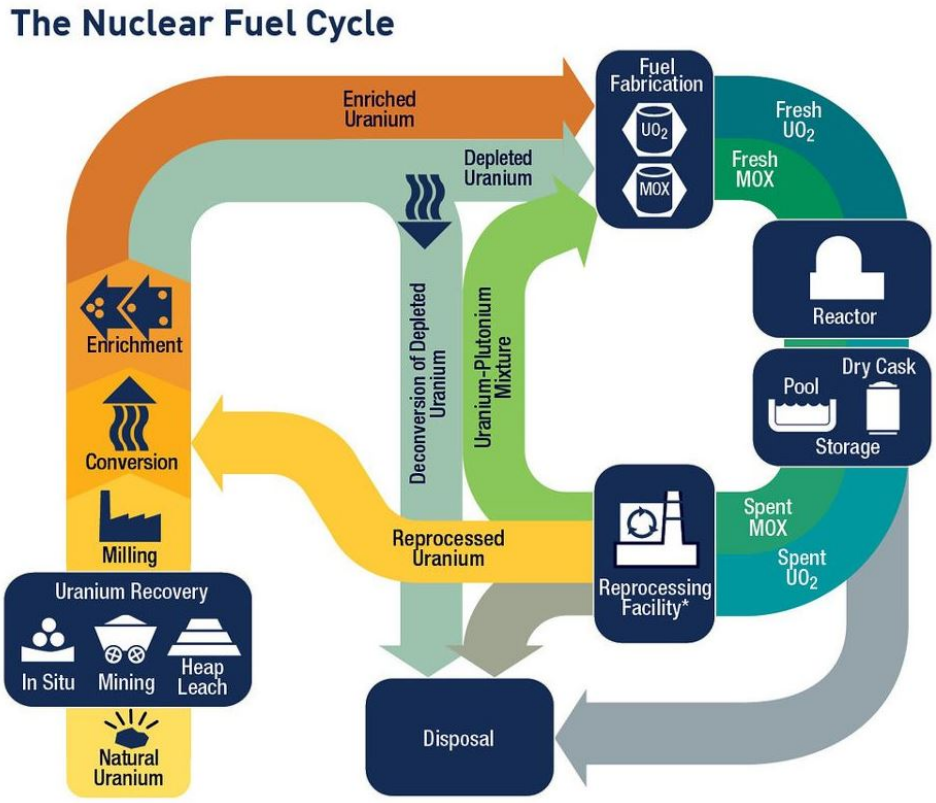

Figure 2.3. The nuclear fuel cycle used for UO_2 and MOX fuels for power production [10]. Source: U.S. Nuclear Regulatory Commission.

The cycle begins with the mining and initial processing of uranium ore [10]. This ore typically contains U_3O_8, or yellowcake, which is chemically separated from other materials left over from the mining and milling processes. The U_3O_8 is then either converted to UF_6 or directly to UO_2 or uranium metal alloy fuel. In the case of direct conversion, the fuel is used in reactors capable of operating with naturally enriched uranium [10]. These reactors feature high neutron economy, such as the Canada Deuterium Uranium reactor (CANDU-6).

If the uranium ore is converted to UF_6, it is to be used in the enrichment process. Uranium enrichment is the process of increasing the concentration of ^{235}U to make it more favorable for reactors with less neutron economy and allow greater extraction of energy per unit mass. The enriched UF_6 is then converted to UO_2 or uranium metal

alloy fuel to be used in a reactor. The leftover depleted uranium, called tailings, is converted back into yellowcake to reduce chemical hazards and sent to disposal.

After the fuel is used in a reactor, it is considered spent fuel and has two options [10]. The first option is to classify it as high-level waste and store it. The second option is to reprocess the spent fuel and extract the remaining uranium and plutonium. The extracted fuel is then used in the enrichment and fabrication processes to make mixed oxide (MOX) fuel. The remainder of the spent fuel after reprocessing is classified as high-level waste and treated the same as in the first option.

2.2.1 Plutonium Production

Some reactors, known as breeder reactors, optimize their operational cycles and and core design for the production of plutonium. They use shorter fuel burn cycles to increase the ^{239}Pu concentration to use in other applications such as weapons. If the fuel burns for too long, it increases the ^{240}Pu concentration, making it not as useful [11].

^{239}Pu is created by a ^{238}U atom that absorbs a neutron and double beta decays. Figure 2.4 shows the ^{238}U capture cross section which can be interpreted as the ^{239}Pu production cross section. ^{239}Pu then has two primary loss mechanisms. The first is fission of ^{239}Pu as it is a fissile element. The second is the further absorption of a neutron and the creation of ^{240}Pu. A breeder reactor will maximize thermal neutrons for the creation of ^{239}Pu but will have shorter operational cycles to limit the amount of ^{240}Pu that is created. The exact time the fuel is removed can be optimized for the desired purpose of the plutonium. Isotope production is further discussed in Section 2.4.3.

Because of the shorter operational cycles, breeder reactors are refueled more frequently. These reactors often simplify the fuel cycle by using natural uranium thereby

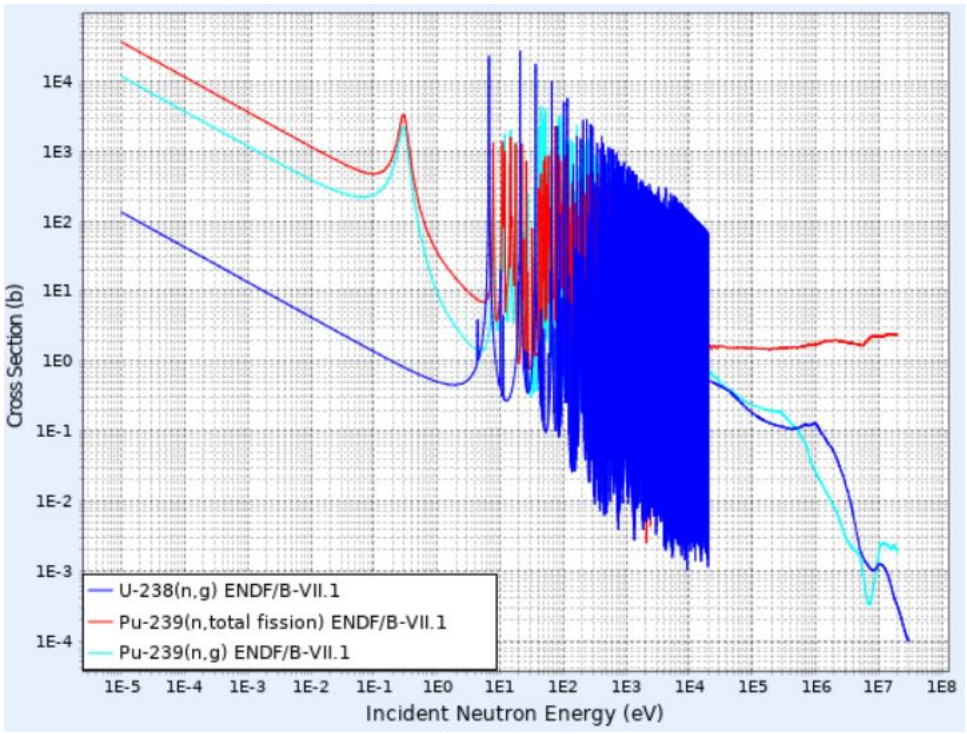

Figure 2.4. Total fission cross-section for ^{239}Pu and absorption cross-sections for ^{239}Pu and ^{238}U using ENDF/B-VII.1 [12].

skipping enrichment. Natural uranium is also a benefit for plutonium production as it has a higher ratio of ^{238}U for creating ^{239}Pu and requires higher neutron economy to maintain criticality [11].

2.3 Nuclear Reactors

2.3.1 Fundamentals of Reactors

Nuclear reactors are systems that utilize nuclear processes to release energy and/or produce radionuclides [13]. The most common type of reactor is the fission reactor, which uses neutrons to "split" fissionable isotopes; usually ^{235}U and ^{238}U. This process results in approximately 200 MeV of energy, depending on the parent isotope, as well as 2-3 neutrons and 2 fission products per fissioned nucleus as shown in Figure 2.5. The excess of neutrons then can cause fission in another ^{235}U or ^{238}U atom thereby

sustaining a chain reaction.

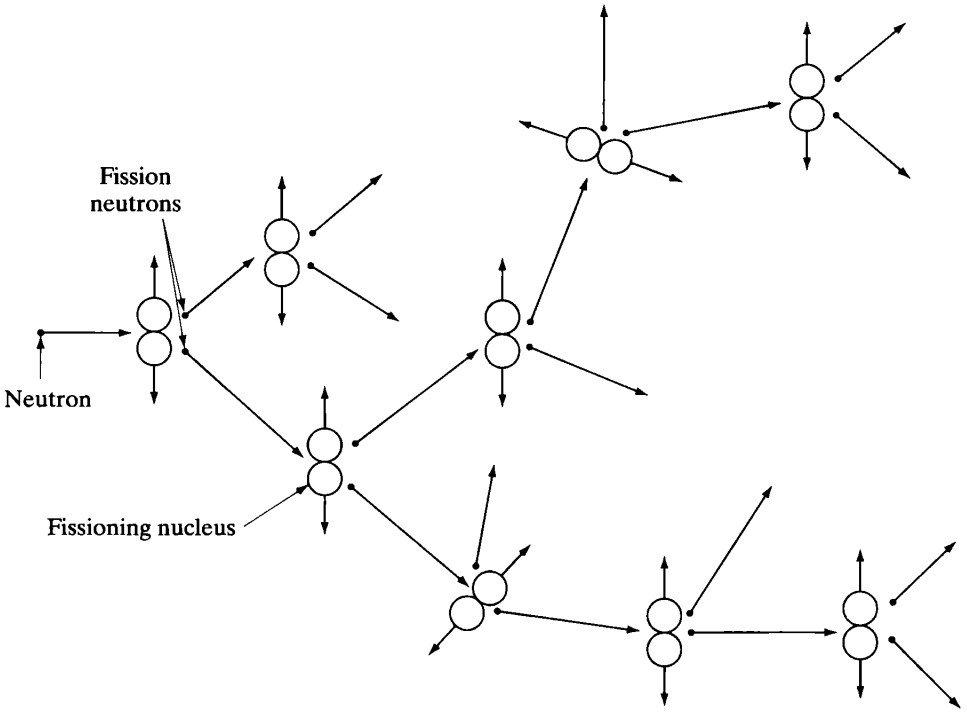

Figure 2.5. Chain reaction of neutrons and fissionable nuclei. In this schematic, each reaction produces two fission products and two neutrons which cause more fission [13].

Neutrons are not limited to inducing fission. They are capable of additional interactions such as scattering or activation. Neutron activation is the absorption of a neutron by a nucleus that produces a new heavier isotope of the same element [13]. For example, a ^{238}U atom can capture a neutron and either fission or become ^{239}U. If unstable, this new isotope can radioactively decay into another isotope.

Each isotope has a different probability, called a cross section, of scattering or absorbing a neutron [13]. This probability has a dependence on incident neutron energy and the cross section of the target isotope. Figure 2.6 displays the fission cross section for ^{235}U in blue and ^{238}U in red as a function of incident neutron energy. The x-axis is the incident neutron energy and the y-axis is the probability the nucleus will capture the neutron and fission.

However, not all neutron captures on uranium lead to fission. For example, Fig-

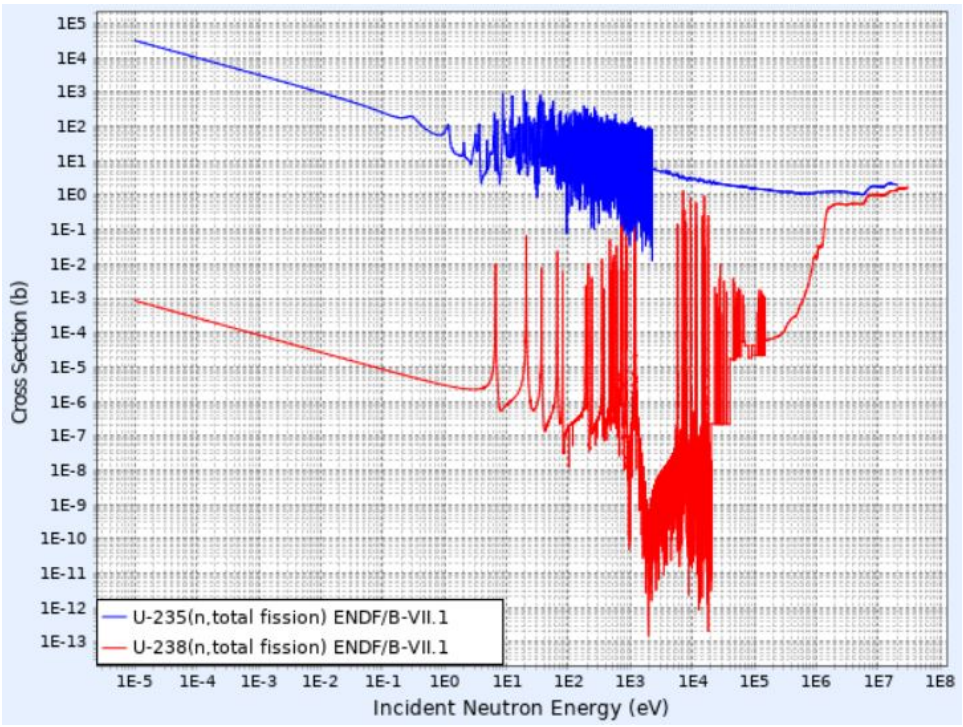

Figure 2.6. Total fission cross-sections for ^{235}U and ^{238}U using ENDF/B-VII.1 [12].

ure 2.7 displays the fission cross section for ^{238}U in blue and the capture cross section in red. Figure 2.7 and Figure 2.6 show the effect neutron energy has on reaction probabilities and isotope production.

Differences in reaction cross sections are the reason behind reactor core and fuel loading pattern design [13]. Uranium fuel is often enriched in the nuclear fuel cycle to leverage the higher fission cross section in ^{235}U versus ^{238}U. To further leverage interaction probabilities, neutrons are "slowed down" with the use of a moderating material, such as water, heavy water, or graphite, because ^{235}U has a higher fission cross section for lower energy neutrons as shown in Figure 2.6. Fuel type, enrichment, and moderating materials are only a few of several factors that contribute to a successful reactor design, and each of these factors will create an unique neutron spectrum resulting in varying radioisotope production.

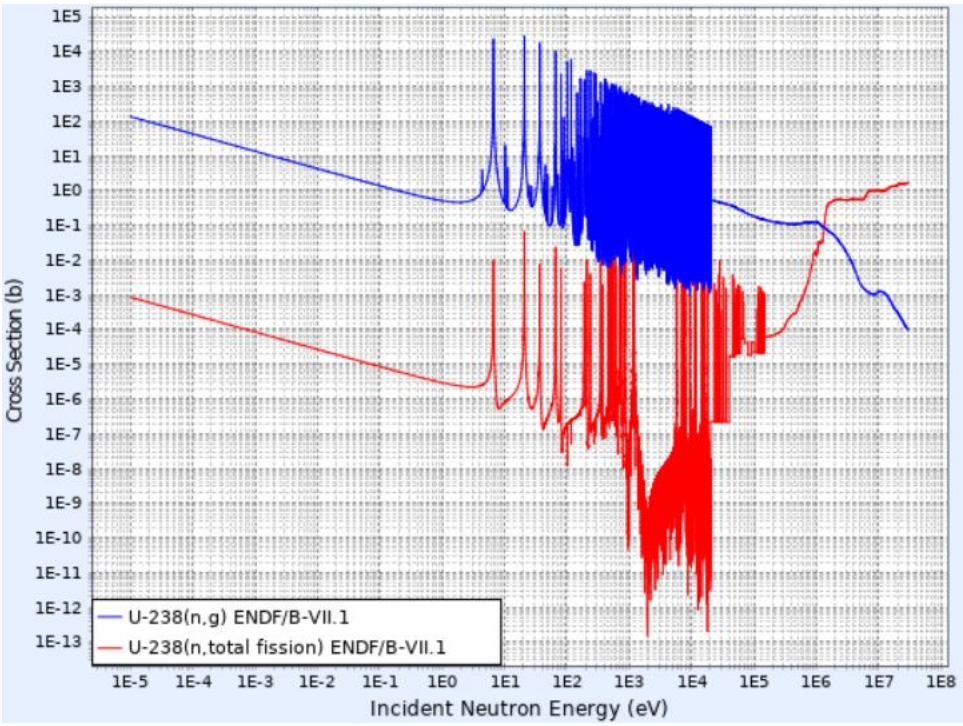

Figure 2.7. Total fission and neutron capture cross-sections for ^{238}U using ENDF/B-VII.1 [12].

2.3.2 Reactor Classes

Power Reactors

The most common application of nuclear reactors is for power production. NPPs use the energy released by fission to heat coolant that drives a turbine for generating electricity. These reactors all use the same fundamental principles, but are separated into six distinct classifications based on their fuel structure, moderator, and coolant [14].

The Magnox and Advanced Gas-Cooled Reactors (AGR) are two of the oldest commercial reactor designs. Both designs utilize carbon dioxide gas as coolant and graphite as moderator, but that is where the similarities end [14]. Magnox uses natural uranium metal as its fuel with magnesium alloy as cladding. Magnox reactors are still used today; however, they lack thermal efficiency compared to AGRs. AGRs

are an improvement over Magnox reactors because they use 2.3% enriched UO_2 fuel with stainless steel cladding instead of uranium metal. This allows them to operate at much higher temperatures and pressures, which increases the thermal efficiency from 31% to 42%.

Canada Deutrium Uranium (CANDU) reactors are a popular design that does not require enrichment of the fuel. CANDU reactors use naturally enriched UO_2 fuel with zirconium alloy cladding [14]. CANDUs are capable of using natural UO_2 because of the neutron economy benefits of heavy water moderator and coolant. The CANDU-6 design is further discussed in Section 2.3.3.

The most widely used reactor designs in the world are the Pressurised Water Reactor (PWR) and the Boiling Water Reactor (BWR) [14]. These designs are popular because they use ordinary water as both moderator and coolant. They are able to use ordinary water because their fuel is 2%-5% enriched UO_2. This additional enrichment compensates for the loss in neutron economy from absorption loss in ordinary water compared to heavy water. The primary difference in BWRs and PWRs is how they convert heat into electricity. The BWR is considered a low pressure system as it boils its water to produce steam to drive the turbines in a single loop. The PWR is operated at high pressure thereby prohibiting phase change of the water coolant in the primary loop. The heated water is then used to boil water in a secondary loop.

The last of the six core commercial reactor designs is the RBMK [14]. The RBMK is most commonly used within Russia and the surrounding countries that formerly made up the USSR. It uses 1.8% enriched UO_2 fuel with a graphite moderator and light water coolant. The RBMK is the design of the Chernobyl reactor that exploded in 1986.

Isotope Production and Research Reactors

Isotope production and research reactors are smaller scale reactors designed for purposes other than power generation. They are usually lower power reactors that leverage high neutron flux with strong moderation to maximize neutron absorption in target materials [15]. A common application of this type of reactor is for the production of medical isotopes. These isotopes are used in a variety of applications including radiation therapy, tracers, pharmaceuticals, and more. Radioisotopes are also created for research and/or technology with other purposes. For example, ^{241}Am is a commonly used alpha particle source, and the Mars Rover was powered by a small radioisotope reactor containing ^{238}Pu. Many of these reactors are also classified as research reactors as they have facilities available for ongoing experiments.

2.3.3 CANDU-6 Reactors

The CANDU-6 reactor, the focus of this research and currently the most common CANDU design in the world, is an example of a potentially dual-purpose reactor capable of being used both for isotope production, in this case the production of plutonium, and power [14, 16]. The core design of the reactor is similar to other CANDU designs as it uses naturally enriched UO_2 fuel, covered in zirconium alloy cladding, with heavy water moderation and coolant. A full core contains more than 100 metric tons of fuel and typically produces around 600 MWe of power.

The basic building block of a CANDU-6 core is a fuel bundle, shown in Figure 2.8. Each fuel bundle is approximately 11.2 cm in diameter and 49.5 cm in length and contains 37 fuel pins.

Three-hundred and eighty fuel channels, composed of 12 fuel bundles per channel, are arranged in a cylindrical stainless steel calandria as shown in Figure 2.9. Each fuel channel is filled with heavy water coolant and pressurized within a smaller zirconium

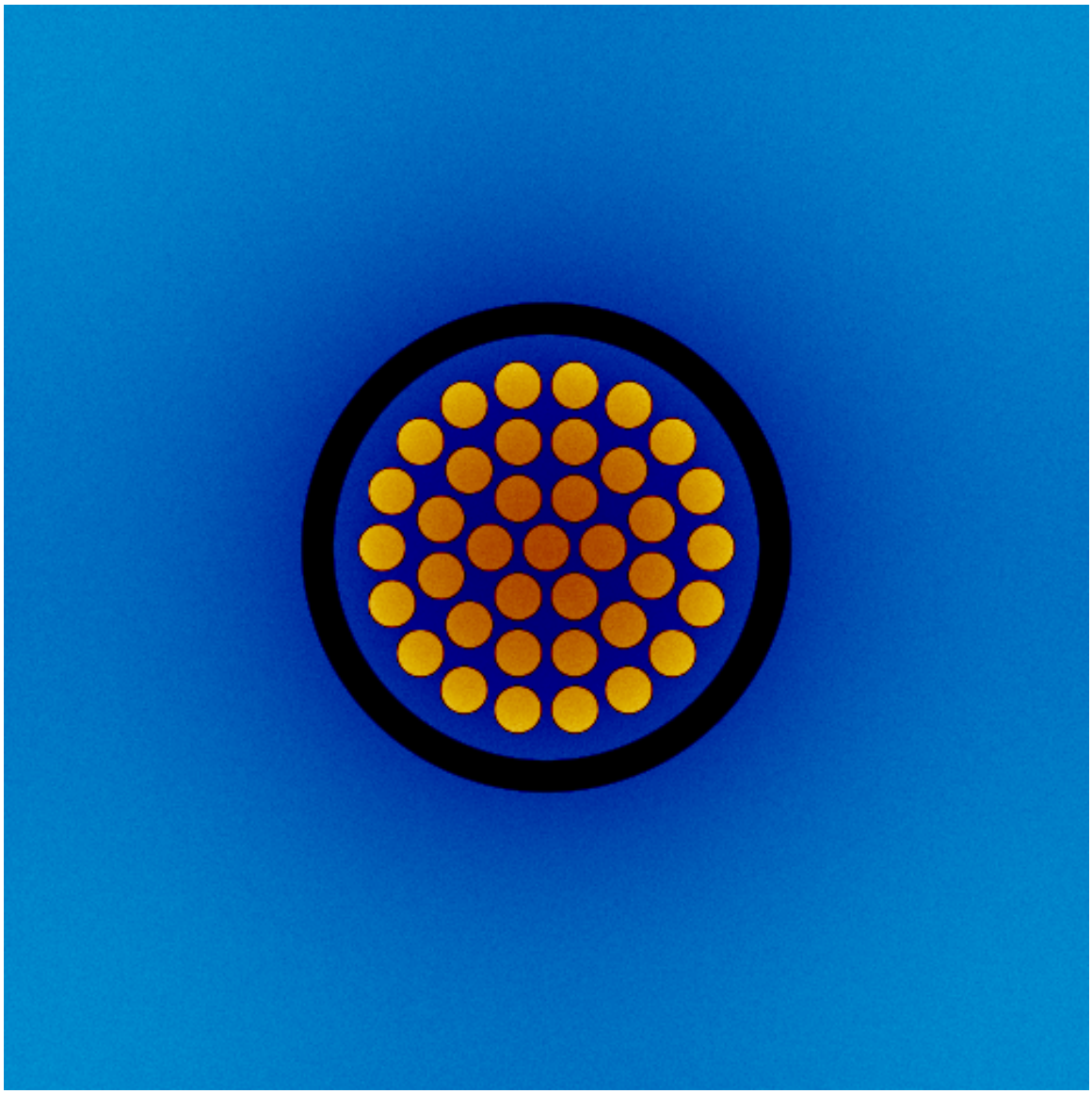

Figure 2.8. Diagram for the 37-pin natural UO_2 CANDU-6 fuel bundle.

calandria. The array of fuel channels is surrounded by lower pressure heavy water inside the steel calandria. Cadmium adjuster rods, not shown in Figure 2.9, are used to control the reactor. The fuel array is surrounded by an average of 65 cm of heavy water moderator and 41.9 cm of calandria tube shielding [7, 16].

A unique capability of the CANDU reactor is its capability to be refueled online [16]. This means it is able to have depleted fuel replaced with fresh fuel without having to shut down the reactor. This is accomplished by maintaining a pressurized system

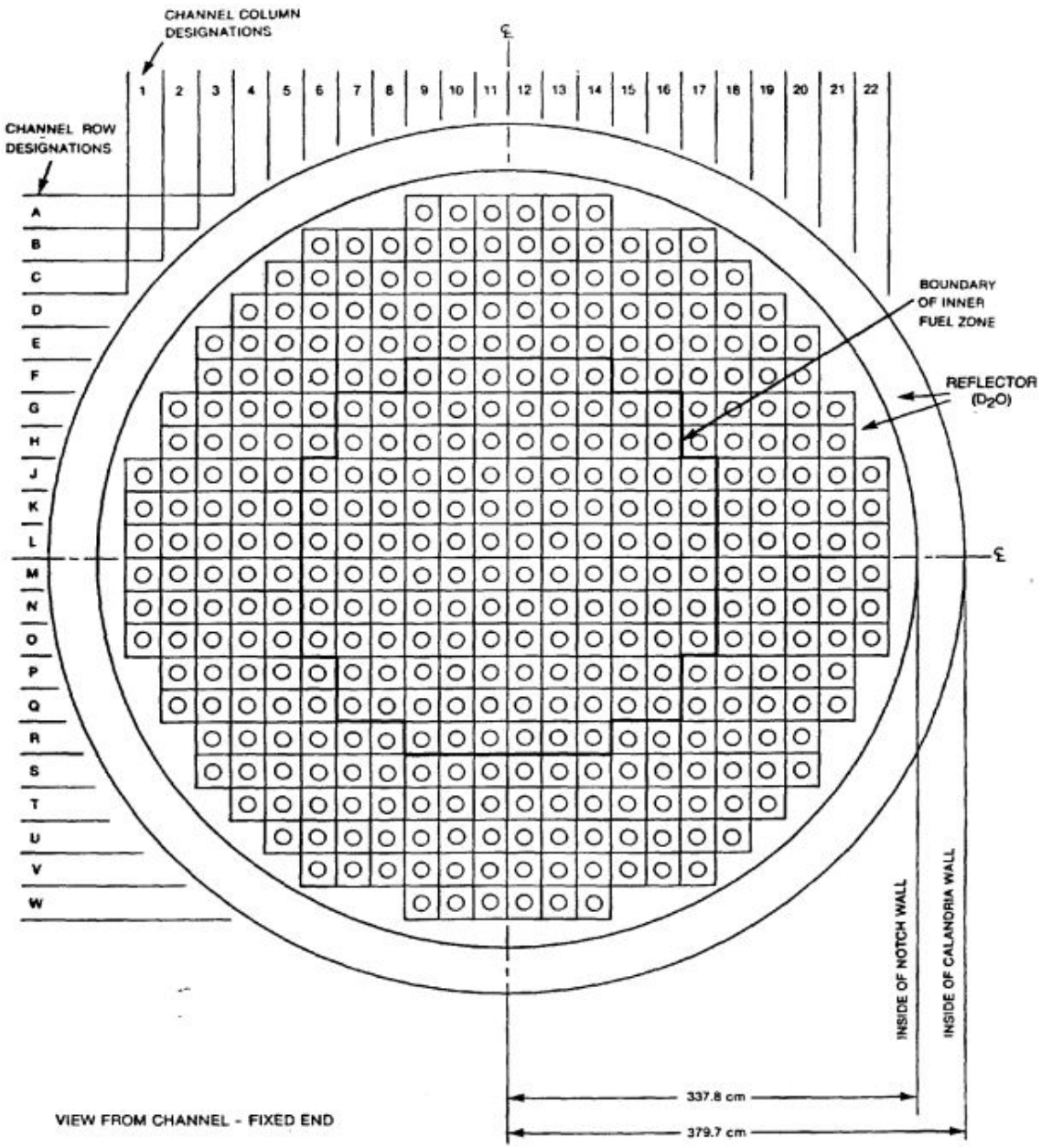

Figure 2.9. Axial schematic for a full-core CANDU-6 reactor [16].

and using the swing-eight refueling scheme shown in Figure 2.10. Three to four times per week, on average, a single fuel channel is selected for refueling and undergoes the swing-eight refueling scheme. First, the two end bundles in the direction of refueling are removed and saved. Then, the center eight fuel bundles are removed and sent to the spent fuel bay. The first two bundles are then replaced in the fuel channel and

pushed to the opposite end. Finally, the fuel channel is filled with eight fresh fuel bundles. The next time this channel is refueled, it is refueled in the opposite direction. This refueling scheme maintains criticality and an even power distribution without the need to shut down. Other refueling methods such as the shift-eight refueling scheme exist; however, this work used the swing-eight refueling scheme [16].

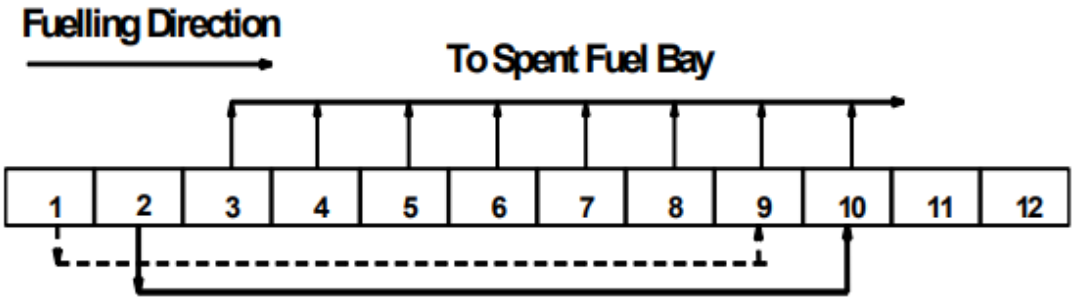

Figure 2.10. The swing-eight refuelling ccheme used for channel refueling in a CANDU reactor [16].

The CANDU-6 reactor is of interest to this work because of its unique capabilities for isotope production and the ability to separate small components of the core. The relatively low burnup for each fuel bundle at the time of refueling for the CANDU-6, necessitated by the use of natural uranium, makes it useful for the production of plutonium and a potential proliferation risk [11]. Therefore, it is important to understand the possible signatures this reactor creates from steady-state operations.

2.4 Reactor Modeling

2.4.1 Serpent 2

Serpent 2 is a multi-purpose three-dimensional continuous-energy Monte Carlo particle transport code developed by Dr. Jaakko Leppänen at the VTT Technical Research Centre of Finland and designed for reactor transport modeling [8]. It began as a simplified reactor physics code, but was expanded to include modern techniques

for neutron and photon transport, criticality calculations, reactor modeling, coupled multi-physics calculations, and burnup. This code was chosen for this research because of its modern implementation of geometry modeling, neutronics, and burnup calculations.

2.4.2 Criticality Modeling

Criticality modeling is the bread and butter of modeling critical reactor systems. These models are used to solve steady-state time-independent problems. Common uses include criticality calculations, criticality optimization, flux and power analysis, particle tallying, safety analysis, and more [8].

Neutronics

Neutron particle transport, also known as neutronics, is broken down into two categories: Monte Carlo and deterministic [13]. Deterministic transport is the method of using analytical techniques to solve the energy, space, angle, and time dependent transport problem. For reactors, this is the solving of the time-independent Boltzmann Transport Equation (BTE), which is given as

$$\begin{aligned} \Omega \cdot \nabla \Phi(r, E, \Omega) = -\Sigma_t(r, E)\Phi(r, E, \Omega) + \frac{1}{4\pi} S_f(r, E) \\ + \int_{\Omega'} \int_{E'} E_S(r, E' \rightarrow E, \Omega' \rightarrow \Omega)\Phi(r, E', \Omega') dE' d\Omega' \end{aligned} \tag{2.1}$$

where

$\Omega \cdot \nabla \Phi(r, E, \Omega)$ is the migration term,

$\Sigma_t(r, E)\Phi(r, E, \Omega)$ is the neutron loss,

$\frac{1}{4\pi} S_f(r, E)$ is the fission source,

and

$\int_{\Omega'} \int_{E'} E_S(r, E' \rightarrow E, \Omega' \rightarrow \Omega)\Phi(r, E', \Omega')dE'd\Omega'$ is the scattering source.

Different forms of the BTE can be formulated to solve using either integral, differential, or integro-differential methods [13]. The accuracy of deterministic methods are limited by the discretization of the phase space. For multi-scale geometries like the CANDU-6 reactor, this can be a limiting factor as the geometry is only approximately represented or a large amount of memory is required to store what can be trillions of variables.

In contrast, Monte Carlo transport is the stochastic, or probabilistic, method of solving a transport problem. In Monte Carlo transport, the geometry and materials can be exactly represented, but the particle interaction and transport is sampled from expected probability distributions. This method closely represents the real, stochastic behavior of particles moving throughout a medium. However, because Monte Carlo is probabilistic, statistical variance exists in the results. As the sample size increases, the result approaches the true population results according to the Central Limit theorem. In other words, the precision of the result can always be improved with more sampling given the computational resources needed. This makes it an excellent choice for large, complex, multi-scale systems, but it is generally computationally intensive, which can result in moderate uncertainties in less sampled regions of the problem. Monte Carlo neutron transport is used in this research because of its ability accurately represent a given system and the advanced techniques Serpent 2 offers such as Woodcock delta-tracking that reduce the computational requirements [8].

Particle tracking in Monte Carlo transport is performed through either surface-tracking or Woodcock delta-tracking [17]. Surface-tracking is the conventional method that evaluates the particles next interaction probability at each surface or boundary crossing. This can be a very computationally intensive method for systems where

the expected distance a neutron travels, or the neutron mean free path, is long compared to the dimensions of the geometry. This is especially true for nuclear reactors featuring millions of unique surfaces. To combat this, the Woodcock delta-tracking method was developed in 1965 [18]. Instead of re-sampling every time a surface is encountered, Woodcock delta-tracking uses all of the materials within the mean free path of a neutron and calculates a new mean free path based on those materials [17]. Specifically, a majorant cross section, Equation 2.2, is calculated and used to track virtual collisions.

$$\Sigma_{maj}(E) = max\{\Sigma'_{tot,1}(E), \Sigma'_{tot,2}(E), ..., \Sigma'_{tot,M}(E)\} \tag{2.2}$$

Virtual collisions allow the tallying of interactions without changing the energy or direction of the neutron. Then, rejection sampling is used for each virtual collision to determine if it is accepted as shown in Equation 2.3. This results in re-sampling only occurring when a neutron encounters an accepted interaction rather than at every surface [17].

$$P_m(E) = \frac{\Sigma_{tot,m}(E)}{\Sigma_{maj}(E)} \tag{2.3}$$

Woodcock delta-tracking loses efficiency when a neutron encounters a material that causes a strong gradient in neutron flux such as a control rod [17]. The loss in efficiency is due to the excessive virtual collisions that fail when the majorant cross section is large, but the current material cross section is small. Serpent 2 uses both techniques to improve performance by using the faster Woodcock delta-tracking method for the majority of interactions. When encountering materials such as control rods, Serpent calculates the sampling efficiency of Woodcock delta-tracking and switches to surface tracking when the efficiency meets a predetermined cutoff,

c. The switch from delta-tracking to surface-tracking is made when the condition in Equation 2.4 fails.

$$\frac{l_{maj}(E)}{l_m(E)} = \frac{\Sigma_{tot,m}(E)}{\Sigma_{maj}(E)} > 1 - c \tag{2.4}$$

Cross sections

Nuclear reaction cross sections are the probability that a given nuclear reaction will occur [12]. They make up the core data structure that neutronics calculations use [8]. This research used the Evaluated Nuclear Data File B-VII.1 (ENDF/B-VII.1), a standard for evaluated cross-section data for simulating thermal fission reactors [12]. ENDF/VIII was not used because of its unavailability at the start of this work.

Complex neutronics calculations, such as a nuclear reactor, use thousands of cross-sections for the different materials. In general, there is one cross section per discrete material temperature, per reaction, per isotope. This creates a large memory and computational speed problem for complex systems. Serpent 2 implements the use of a unionized energy grid to combat this while still maintaining accurate results [19]. During pre-processing, the continuous-energy cross-sections for all materials are read and reconstructed into a single unionized energy grid. This removes the need to access the raw cross-section data from library files mid-transport cycle but increases the required memory. To reduce the amount of required memory, energy grid thinning can be used to apply an energy binning tolerance and reduce the number of data points. Serpent reconstructs its energy grid with grid thinning by keeping points deemed important, such as local minima and maxima, and combining adjacent points based on a user defined fractional tolerance as shown in Equation 2.5. Results are not significantly affected up to a tolerance of 1e-3 [8].

$$\frac{E_j - E_{j-1}}{E_{j-1}} < \tau \tag{2.5a}$$

$$E'_{j-1} = \frac{E_j + E_{j-1}}{2} \tag{2.5b}$$

Evaluated nuclear cross-section libraries such as ENDF/B-VII.1 are not exhaustive and complete. For example, they are discretized to select material temperatures, typically intervals of 300K and often lack resolution in resonance regions [8]. Serpent 2 utilizes built-in functions to fill in these gaps. For material temperatures, a doppler-broadening rejection-correction pre-processor can be used to adjust cross-section data to the correct temperatures [8, 20]. Zero-Kelvin cross-section data are used in this temperature correction. For unresolved resonance regions, which are overlapping data points in high energy resonances, another pre-processor correction can be applied to interpolate or average values to increase accuracy.

2.4.3 Burnup Modeling

When steady-state time-independent results from criticality modeling are not sufficient and results due to transient effects are required, burnup modeling is employed [8]. Burnup modeling is the use of neutronics results from a criticality model to solve for the changes in materials due to isotope production and decay. This production and decay process is captured by the Bateman equations, shown in Equation 2.6. The new materials obtained from the Bateman equations are used in the criticality model to obtain the neutronics results at each different timestep. Due to the range of isotope half-lives, the selection of timesteps to account for the rapid in-growth and decay of short-lived isotopes while reducing computational costs becomes an important factor.

$$\frac{dN_1(t)}{dt} = -\lambda_1 N_1(t) \tag{2.6a}$$

$$\frac{dN_i(t)}{dt} = -\lambda_i N_i(t) + \lambda_{i-1} N_{i-1}(t) \tag{2.6b}$$

$$\frac{dN_k(t)}{dt} = -\lambda_{k-1} N_{k-1}(t) \tag{2.6c}$$

The actual implementation of the Bateman equations in reactor burnup modeling is more complicated as there are more channels for isotope production and loss due to the neutron flux. Equation 2.7 shows the isotope production rate of isotope i inside a nuclear reactor [13]. The first term on the right hand side of Equation 2.7 is the production rate of isotope i from fission. This is a fraction of the total fission rate denoted by γ_i. The second term is the production rate of isotope i by neutron interactions with other isotopes. This reaction channel is most commonly neutron absorption (n,γ), but can be other reactions, such as (n,2n), where a neutron is knocked out of the target nucleus. The third term is the loss rate of isotope i by neutron interactions. The fourth and fifth terms are the respective production and loss rates from radioactive decay. These production and loss channels are used together to calculate the change in isotopic concentrations over a given timestep.

$$\frac{dN_i(t)}{dt} = \gamma_i \Sigma_f(E,t)\Phi(E) + \Sigma_j(E,t)\Phi(E) - \Sigma_{i,a}(E,t)\Phi(E) + \lambda_p N_p(t) - \lambda_i N_i(t) \tag{2.7}$$

Solving the Bateman equations is a particular challenge as each timestep is usually paired to another neutronics calculation, which rapidly increases required computational time [8]. To reduce the number of required timesteps for convergence, different solving algorithms are applied. The first algorithm implemented in this research is the higher order predictor-corrector calculation [21]. The predictor-corrector method

of solving the Bateman equations uses the results of the first neutronics calculation as a constant to extrapolate for the change in materials for a second neutronics calculation. Then, the results of the second calculation are used to linearly interpolate back over the burnup step to correct for inconsistencies. Higher-order refers to the use of linear extrapolation and quadratic interpolation instead of constant and linear, respectively. This allows the use of the previous burnup step results, which increases accuracy and reduces the required number of burnup steps. Isotalo, et al. tested five combinations of extrapolation and interpolation and found linear extrapolation clearly improved the results for long-lived nuclides [21]. Using linear extrapolation and quadratic interpolation helps reduce the number of burnup steps required to obtain accurate results which reduces overall computational requirements.

The second algorithm implemented is the Chebyshev Rational Approximation Method (CRAM) [22]. CRAM splits each burnup step into smaller substeps and solves them sequentially. This helps account for the rapid in-growth and decay of isotopes and increases the performance of linear and quadratic solvers allowing longer burnup steps. Isotalo, et al. found the increased number of substeps from the CRAM method improves the short-lived nuclides results, especially when coupled with quadratic interpolation [22]. Using CRAM with higher order methods further reduces computational requirements for obtaining accurate results.

III. Methodology

There are two methods to assess the variation in isotopic concentrations in a CANDU reactor: directly measure the concentrations within several bundles of spent fuel or model the reactor and simulate typical operating conditions to obtain spatial estimates. Directly measuring isotopic concentrations from spent fuel is a time consuming and expensive process whereas computational simulation can achieve similar results with a fraction of the time and cost. This study uses the Monte-Carlo reactor transport code Serpent 2 to model a CANDU quarter-core and simulate the burnup of its fuel over two complete refueling cycles of the reactor. Due to the complexity of CANDU reactors, additional steps are taken to obtain accurate results and limit the number of assumptions used. This chapter describes the development of the base criticality model in Section 3.1, the implementation of fuel burnup in Section 3.2, and the analysis methods used in Section 3.3.

3.1 CANDU Criticality Model

The CANDU reactor model used in this research is built using the Serpent 2 universe based method. This allows development of the full model using fuel bundles as the fundamental unit. Utilizing this method, fuel bundles can be easily moved for refueling with minor changes to the overall model.

3.1.1 Reactor Materials

The fuel for the quarter-core starts as natural UO_2. The fuel cladding is zirconium alloy, and a void is issued for the air gap between the fuel and cladding. The the fuel channel and core calandria and pressure tubes also consist of zirconium alloy. Two different density heavy water materials are used for the moderator and coolant. The

higher density heavy water (9.646×10^{-2} atom/b-cm) fills the pressure tubes as coolant while the lower density heavy water (7.288×10^{-2} atom/b-cm) fills the remainder of the core as moderator. The adjuster rods are made of AISI type 304 stainless steel. The fuel is the only material in the model permitted to change due to burnup.

All materials used ENDF/B-VII.1 evaluated cross-section data [12]. This cross-section data was used in Serpent's unionized energy grid with a grid thinning fractional tolerance of 5e-5 to improve performance and reduce memory consumption. Doppler broadening rejection and unresolved resonance corrections were applied to uranium and plutonium isotopes. Serpent's default surface-delta tracking method was used for cross-section sampling with the recommended probability threshold of 0.9.

3.1.2 Geometry

The geometry of the CANDU criticality model is built using the fuel bundle as the fundamental unit. Each fuel bundle consists of 37 fuel pins in a cylindrical pattern surrounded by a pressure tube and a calandria tube. The fuel pins are cylindrical with a radius of 0.6103 cm and are surrounded by zirconium cladding 0.0419 cm in thickness [7]. The 37 pins are arranged in four rings with the third ring offset by 15° to match the CANDU fuel bundle design as shown in Figure 3.1. A complete fuel bundle is 49.53 cm in length with a square pitch of 28.575 cm.

A quarter-core model is used due to the quarter-core symmetry of CANDU reactors. This significantly increases computational performance as less memory and lower neutron populations are required for a high fidelity model. The planes corresponding to 270 and 0 azimuthal degrees from the origin, shown in Figure 3.2, were set as reflective boundaries to imitate a full core geometry. The planes for the axial end-caps and the parallel planes to the described reflective planes were set as vacuum

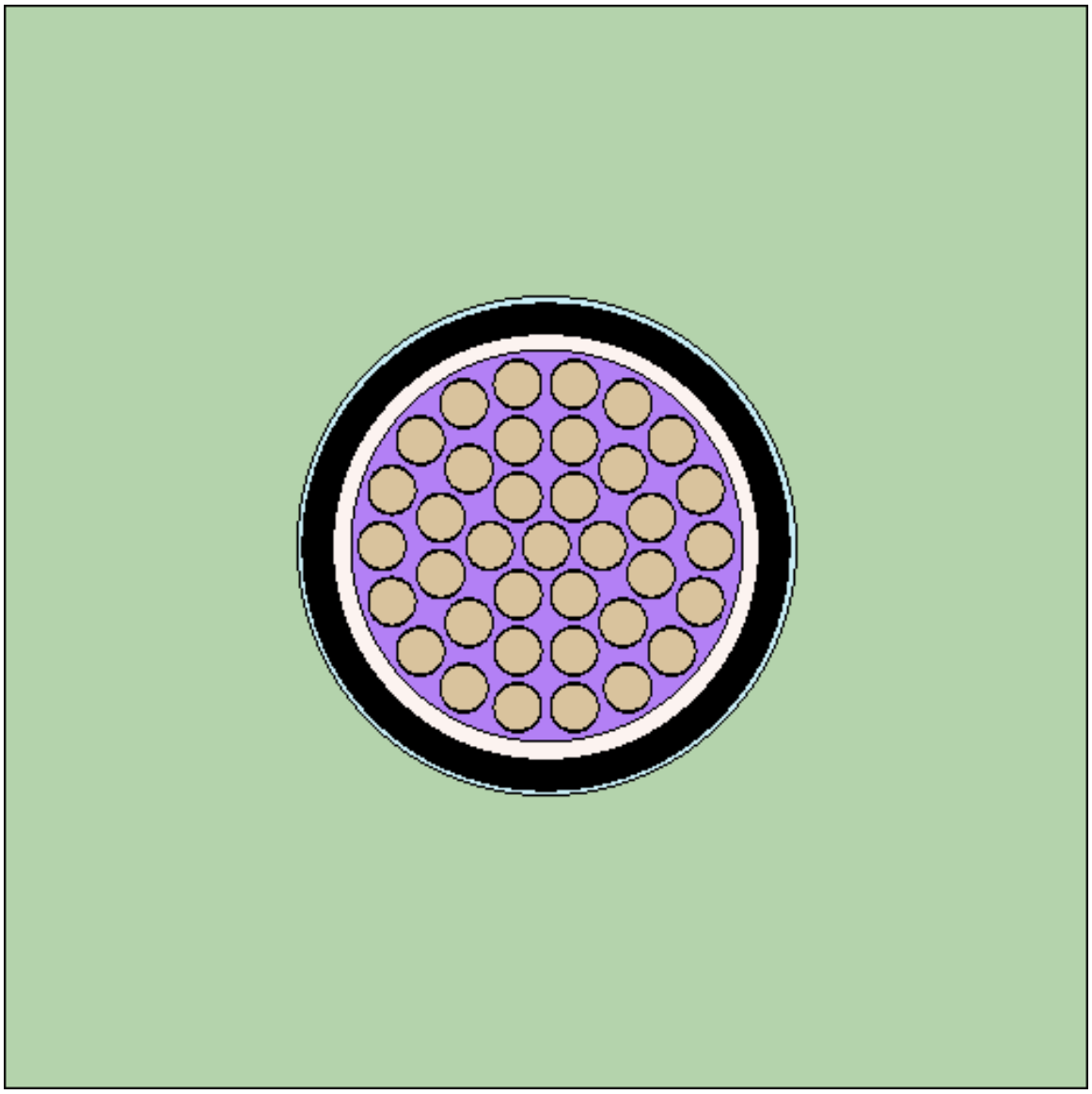

Figure 3.1. CANDU fuel bundle in the z-plane. All fuel bundles utilize this geometry. The orange is the fuel; purple and green are the high and low density moderator, respectively; white is the pressure tube; light blue is the calandria tube; and black is vacuum. Vacuum was used instead of low density gas as the difference in this model is negligible [7].

boundary conditions to prevent unrealistic reflection back into the system. This vacuum boundary assumption slightly underestimates the neutron reflection in the axial directions, but is considered negligible and is consistent with literature [7, 16].

Each fuel channel is 594.36 cm in length and contains twelve fuel bundles. The fuel bundles are placed in a 11×11 quadrant grid consisting of 95 fuel channels as depicted

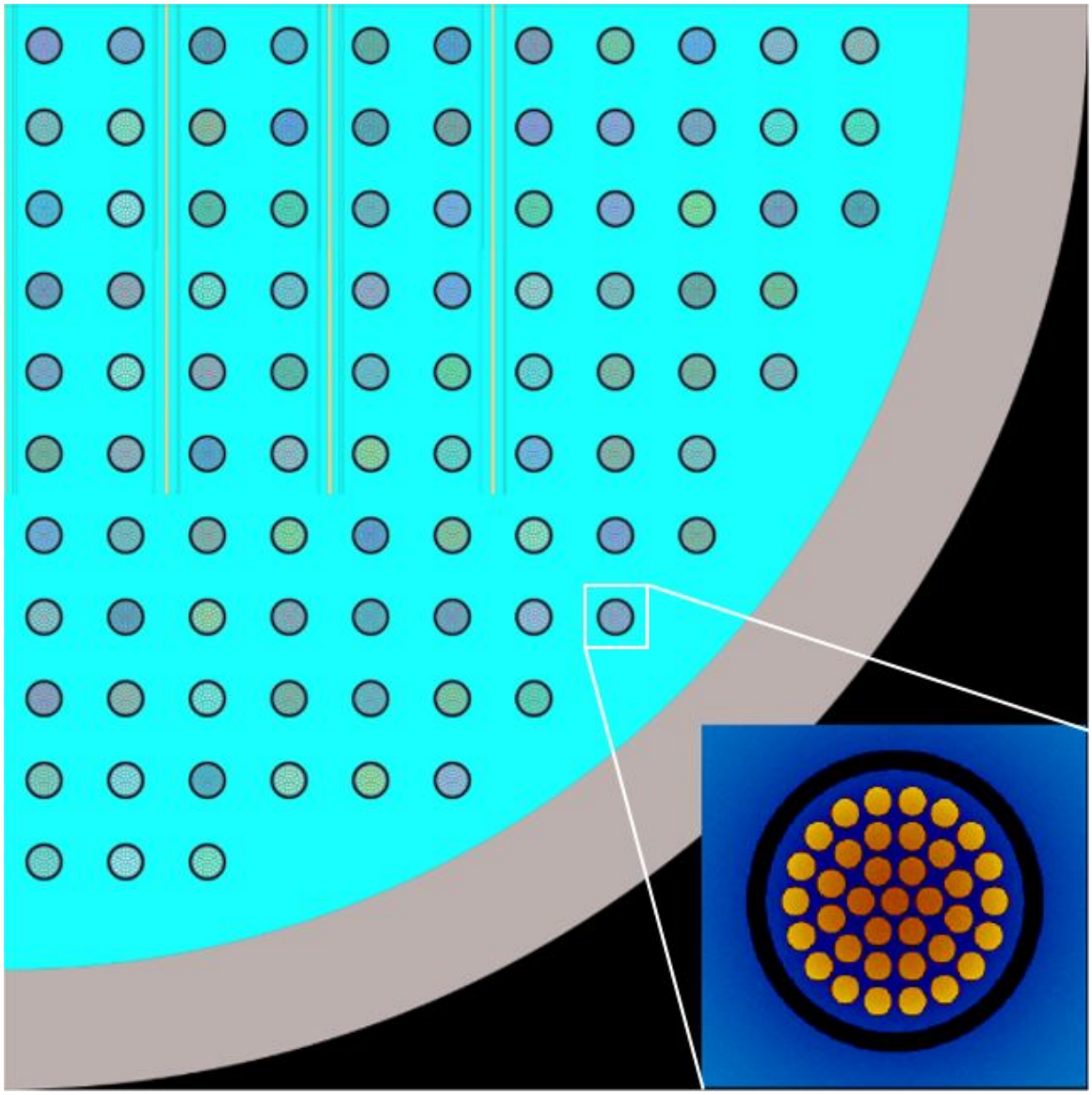

Figure 3.2. An axial view of the quarter-core CANDU-6 model showing the fuel array, structure materials, and adjuster rods.

in Figure 3.2. This results in the quarter-core model containing 1140 fuel bundles. The 11×11 grid is surrounded by an average of 65 cm of heavy water moderator and 41.9 cm of calandria tube shielding in the radial direction. There is no additional moderation or shielding in the axial direction [7, 16].

The adjuster rods, the CANDU equivalent of control rods, are arranged in three rows located at 217.49, 297.18, and 377.18 cm from the axial end of the core [7].

Each row consists of three and a half rods inserted 171.45 cm into the core. The rods are split up into two regions, upper and lower, corresponding to the dimensions in Table 3.1. Heavy water fills any gaps between each region.

Table 3.1. Adjuster rod dimensions for CANDU-6 reactors [7].

	Upper Region (cm)	Lower Region (cm)
Shim Outer Radius	0.650	0.710
Steel Tube Inner Radius	3.607	3.607
Steel Tube Outer Radius	3.725	3.690
Guide Tube Inner Radius	4.519	4.519
Guide Tube Outer Radius	4.572	4.572

3.1.3 Initial Fuel Loading Pattern

The initial fuel loading pattern consists of fresh fuel bundles artificially depleted to the burnup steps listed in Table 3.2. These initial conditions allow a starting point for the burnup model that skips over the complicated CANDU startup process. Realistic reactor startup uses mostly fresh fuel in the majority of the reactor with a few selectively placed depleted fuel bundles [16]. Soluble boron is also used to lower the reactivity until the refueling process can begin. Refueling begins after the fresh fuel has reached peak plutonium concentration and reactivity starts to drop. The plutonium peak is when the ^{239}Pu concentration reaches a maximum and starts being used faster than it is produced. This artificial burn is required because a loading pattern consisting entirely of fresh fuel would be supercritical, data for selectively placed depleted fuel was unavailable, and a realistic startup would add unnecessary complexity to the model.

To obtain the pre-burned fuel bundles, a single fresh fuel bundle was modeled with periodic boundary conditions to simulate an infinite lattice and burned to the eight target burnups. A power density of 21.34 MW/MTU was used to match the average

Table 3.2. Fuel burnups used in the initial fuel loading pattern. The index corresponds to the fuel bundles in Table 3.3 and Appendix A [7].

Index	Burnup (MWd/MTU)
1	32.69
2	78.38
3	342.37
4	818.87
5	1638.73
6	3608.15
7	6381.44
8	8721.49

power density of the full model. Each target was reached using Serpent's burnup mode with the Linear-Extrapolation/Quadratic-Interpolation Predictor-Corrector scheme and 16 CRAM substeps. One thousand active generations and one hundred inactive generations of 10,000 neutrons each were used for each neutronics cycle. These numbers of neutrons and neutron generations were used to obtain negligible uncertainty for the single bundle burn while requiring minimal computational resources. The isotopic concentrations at each burnup target were then used for the eight artificially burned bundles used to construct an initial quarter-core model.

The eight fuel bundles were then placed in the 11×11 grid depicted in Table 3.3 for axial layer 1 of 12 in the CANDU model. Each layer represents the fuel bundle at that axial location. The remaining axial layers are included in Appendix A. The indexing used in Table 3.3 corresponds to the index used in Table 3.2 [7].

This coarse eight-binned fuel burnup structure injects uncertainty into the model but provides a critical starting point for the system. With these initial conditions, injected uncertainty can be removed from the model through the burnup and refueling techniques described in Section 3.2.

Table 3.3. CANDU-6 axial layer 1 initial burnup fuel loading pattern [7].

	A	B	C	D	E	F	G	H	I	J	K
A	7	5	8	3	7	5	8	4	7	4	7
B	5	8	4	8	4	7	4	5	4	7	3
C	7	3	7	5	8	5	7	5	8	1	8
D	5	8	2	8	5	7	5	7	5	7	
E	8	3	7	3	8	4	7	3	7	4	
F	5	8	5	7	5	7	4	7	4		
G	7	4	8	4	6	3	7	4	7		
H	1	7	1	7	4	7	4	8			
I	7	3	7	3	8	2	7				
J	3	7	4	7	3	7					
K	7	4	7								

3.1.4 Criticality Run Conditions

The complete quarter-core model was run with a power density of 21.34 MW/MTU. Two thousand active generations with 250 inactive generations of 200,000 neutrons each were used for the neutronics calculation. The full model required significantly more neutrons compared to the single bundle burn due to the larger scale of the model. These numbers were selected to minimize required computational resources while maintaining adequate uncertainty during testing. Further details are discussed in Section 4.1. To determine the flux variation across the core, flux detectors were used in the most bounding fuel bundles: AA7 and KA1. For channel and bundle identification, the first letter corresponds to the channel column, the second letter corresponds to the channel row, and the number corresponds to the axial placement of the bundle. These detectors tallied neutrons in 500 equal lethargy bins for flux energy spectrum analysis. A fission heat deposition detector was also used to monitor the integrated power in each channel. This provided a quarter-core power profile as shown in Figure 3.3 that was used for burnup monitoring.

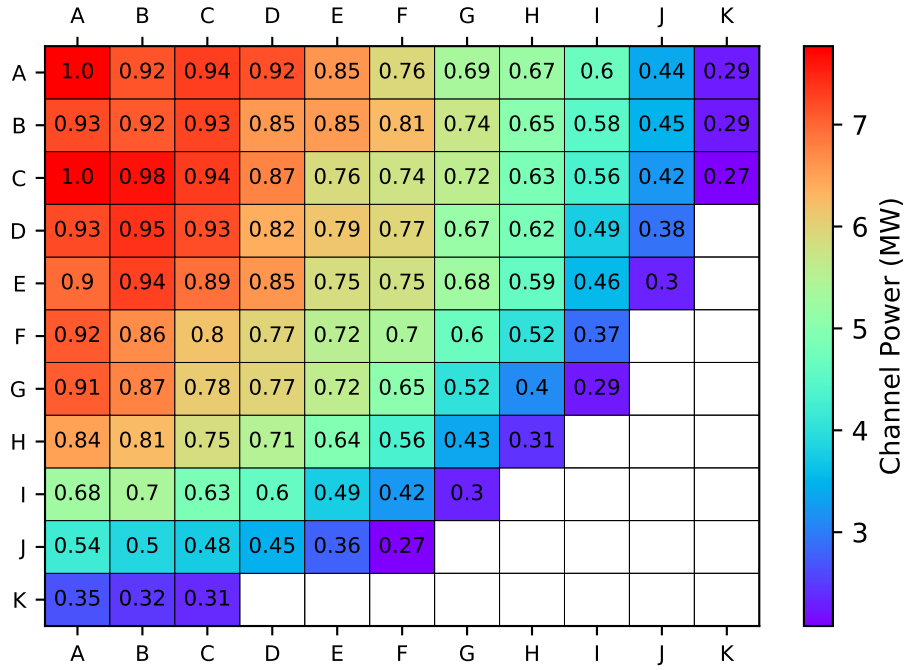

Figure 3.3. Initial power distribution of the criticality model. Channel power values are used to monitor channel average burnup and determine refueling. Overlay values correspond to the channel power normalized to the hottest channel.

3.1.5 Criticality Model Convergence

To ensure the accuracy of the criticality model initial isotopic concentrations, a convergence check was performed on the artificial fuel bundle burn. Figure 3.4 shows the ^{135}Xe concentrations up to their first target, 1.4 days, of the artificial burn using five, ten, and fifteen burnup steps. The first day is the most important in burnup modeling because of the buildup of short-lived fission product poisons. No significant differences were found between the three tests, so five burnup steps were used for the remainder of the artificial burn targets to reduce computational requirements.

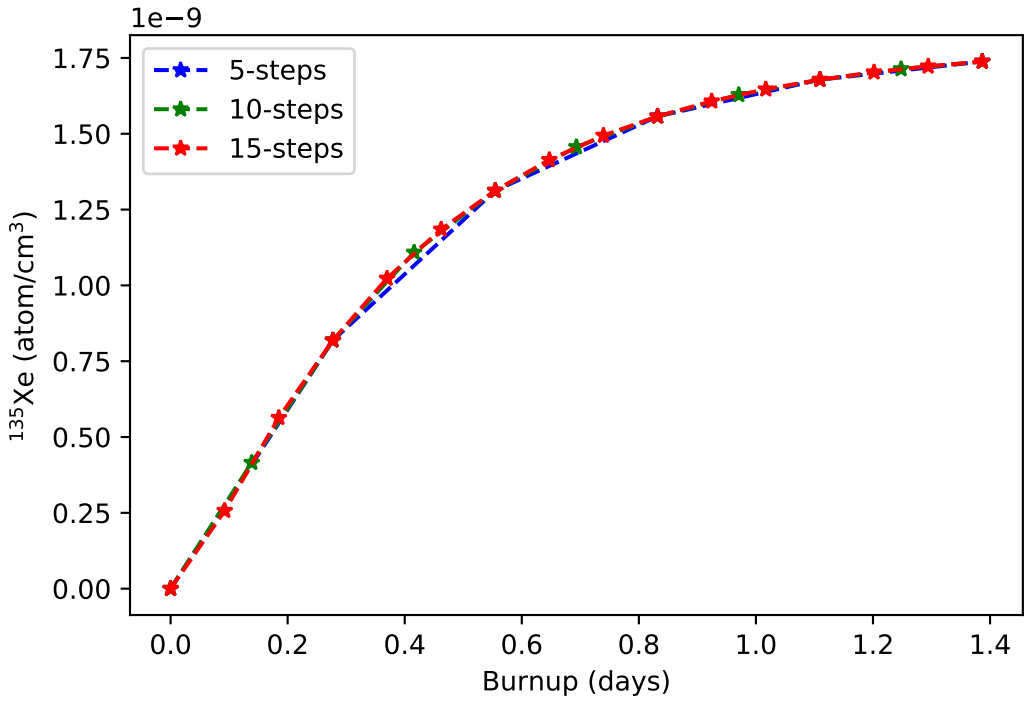

Figure 3.4. Convergence check for the artificial bundle burn. Five, ten, and fifteen burnup steps were used to burn to 1.4 days. No significant differences were found.

3.2 CANDU Burnup Model

3.2.1 Refueling Pattern

A CANDU reactor is capable of online refueling, and it has its fuel changed more frequently compared to other reactors, which adds a level of complexity to the burnup model. To obtain accurate results, this refueling pattern must be preserved in the model. Typically, refueling occurs 3-4 times a week [16]. Using this methodology, a quarter-core burnup model can have one channel refueled every 2.8 Effective Full Power Days (EFPD) to lower the number of required burnup steps.

The selection of channels to be refueled followed a general set of guidelines [16]. Channels were selected based on when they were last refueled, their burnup and power history, and their symmetry within the core. To maintain a consistent refueling

schedule, criteria were established to monitor the model and determine the next channel for refueling. These criteria, listed in Table 3.4, were used to fully automate the burnup model. The criteria for the effective multiplication factor, k_{eff} was used to ensure the model maintains criticality within the reactivity control of the adjuster rods [16]. The burnup limits were used to ensure a channel had been fully burned and had not surpassed its regulated burnup limit of 7.5 GWd/MTU [16].

Table 3.4. Refueling criteria used to automate the burnup model [16].

	Lower Limit	Upper Limit
k_{eff}	0.990	1.010
Burnup	6.5 GWd/MTU	7.5 GWd/MTU

The channel refueling method applied is known as the swing-eight refueling scheme described in Section 2.3.3 [16]. When a fuel channel is selected, the two bundles at the selected refueling side are temporarily removed. Then, the center eight bundles are removed and sent to spent fuel storage. The two bundles temporarily removed are replaced and pushed next to the two bundles at the opposite end of the reactor. Finally, eight fresh bundles are inserted into the empty spots as shown in Figure 2.10. Recursive refuelings of a selected channel followed alternating refueling directions.

3.2.2 Burnup Run Conditions

The burnup model was simulated for a total of 500 refueling cycles to converge the bundle burnup distribution and obtain spent fuel isotopic concentrations for each channel. Each cycle burned the model for 2.8 EFPD, selected a channel for refueling, and refueled the reactor. Isotopic concentrations present in the reactor at the end of each refueling were saved and are documented at the site linked in Appendix B. Appendix C provides an overview of the isotopes tracked that are available from the resources listed in Appendix B.

Three linearly-spaced burnup steps were used for each 2.8 EFPD cycle to solve the Bateman equations using the Linear-Extrapolation/Quadtratic-Interpolation Predictor-Corrector scheme with 16 CRAM substeps. Each neutronics cycle used 1000 active and 40 inactive generations of 100,000 neutrons. Fission source passing was used from one burnup step to the next to reduce the number of inactive generations required for source convergence. These values were selected for the same reasons as discussed in Section 3.1.4.

To determine which channel was ready for refueling, each channel in the model was checked at the end of each burnup step for the criteria listed in Table 3.4. First, the effective multiplication factor was checked to ensure the model was maintaining criticality, 0.99-1.01. Then, if the burnup of the most burned fuel was between 6.5 and 7.5 GWd/MTU, it was selected for refueling; if not, another burnup step was performed to make sure the spent fuel was not removed too early from the reactor. All 500 refueling cycles passed the refueling criteria.

The burnup of each channel is monitored by taking the channel integrated power multiplied by 2.8 days summed over the refueling cycles spent in the reactor. A couple channels close to full burnup in the initial model were analyzed to determine what fraction of burnup is removed when refueling. It was found that it slightly varies channel to channel but averages around 70% of the burnup is removed. A full analysis of the burnup removed could not be performed because burnup was not tracked on a per bundle basis. Therefore, when a channel is selected for refueling, its current burnup is multiplied by 0.3 to account for the bundles that are not removed.

3.2.3 Burnup Model Convergence

The simulation of 500 refueling cycles, equivalent to 1400 EFPD, required further optimization of the burnup methods used to improve computational efficiency and

reduce the computational time required. A technique similar to that used in Section 3.1.5 was used to determine the optimal number of burnup steps to use for each refueling cycle, 2.8 EFPD. Figure 3.5 shows the ^{135}Xe concentrations in bundle AA7 over the first refueling cycle of the burnup model. Six different increments of linearly spaced burnup steps were tested to determine the optimal number of steps to use. All tests returned similar results at the final timestep, 2.8 days; however, the relative difference of these results were compared in Figure 3.6. For each increment tested, the results at 2.8 days were compared to the number of increments before it. As each burnup step approximately increased the run-time of each refueling cycle by one hour, it was imperative to reduce the number required by as much as possible. It was found that using three burnup steps was within 1% relative difference to two burnup steps so three steps was chosen for the remainder of the burnup model refueling cycles.

A convergence check was used to determine when spatial flux, burnup, and isotopic concentration distributions of the burnup model had converged. Figure 3.7 shows the raw $^{239}Pu/^{240}$Pu ratios for the eight spent fuel bundles in all 95 fuel channels. All channels were realigned to show the previous refueling going from the left to the right for the purpose of displaying convergence. For example, bundles 9 and 10 were bundles 1 and 2 in the previous burn cycle and were pushed through with the swing-eight refueling scheme for their most recent depicted burn cycle. From Figure 3.7, it is clear the distribution begins to take shape between 200 and 300 refuelings, indicative of the convergence of the flux and burnup distributions. The remainder of the refuelings were used to update the spatial isotopic concentration distributions using the converged spatial flux. By the time of the 500^{th} refueling, all but 11 out of the 760 fuel bundles had fully converged. These 11 bundles were located in channels near the edge of the core and underwent fewer refueling cycles than the other channels.

Figure 3.8 reinforces Figure 3.7 by showing the $^{239}Pu/^{240}Pu$ isotopic ratio range

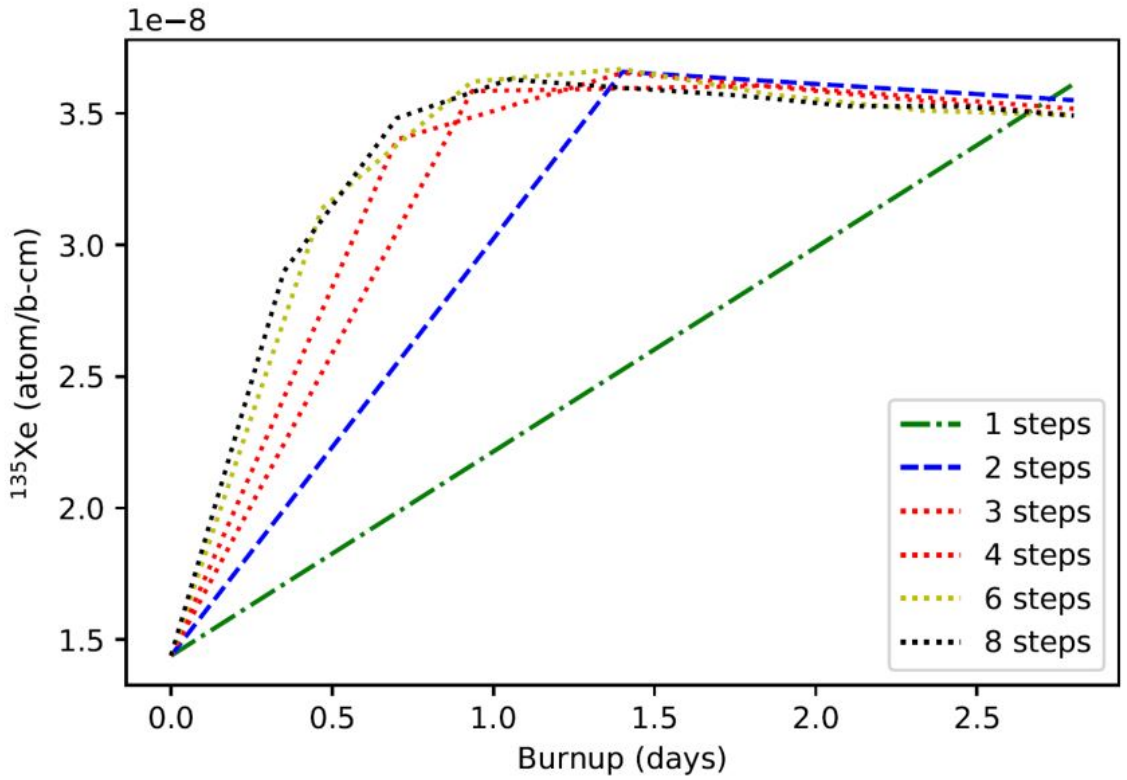

Figure 3.5. **^{135}Xe concentrations in fuel bundle AA7 over the first refueling cycle. Six different linearly spaced burnup increments were tested to build the convergence plot in Figure 3.6**

in spent fuel for bundles 3, 5, 7, and 9 in 25 refueling increments. By the 300^{th} refueling, it is clear that the spatial burnup and flux distributions had converged and the remainder of the refuelings were used to converge the isotopic concentration distributions.

3.3 Spent Fuel Analysis

The selection of fuel bundles for spent fuel analysis followed the methodology of the refueling pattern. The spent fuel analysis was performed on the eight fuel bundles removed from each fuel channel following the swing-eight refueling scheme at the end of their lifetime in the reactor. By selecting these bundles, a radial and axial isotopic concentration profile can be built. This provided a complete picture

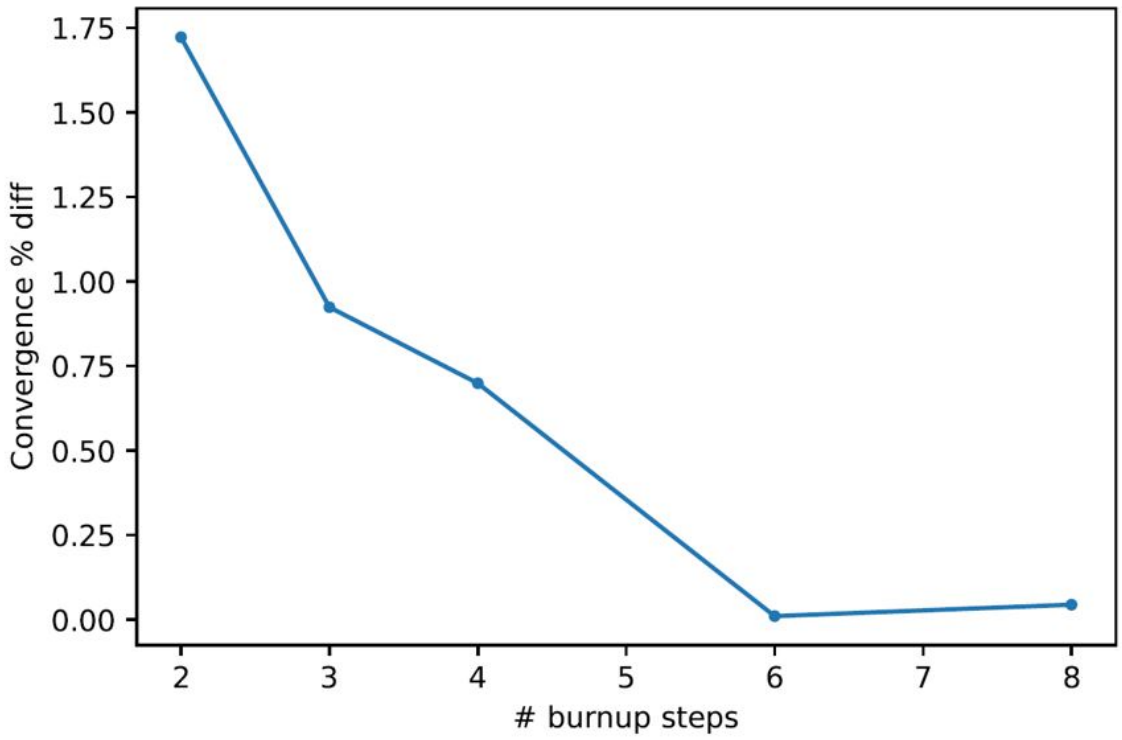

Figure 3.6. Convergence check for the ^{135}Xe concentrations plotted in Figure 3.5. Each point compares the relative percent difference to the point before it.

of the variability in spent fuel by including the entire range of potential burnups and irradiation histories. Concentrations in $(atom/b-cm)$ for 257 isotopes, listed in Appendix C, are stored in a database detailing the isotopic concentration distributions from steady-state CANDU-6 operations.

A subset of these isotopes were selected for further analysis and evaluation. These consist of eight fission products and eight actinides listed in Table 3.5. These selected isotopes are not the only potential signatures of interest to the CTBTO, but they are meant to be representative of the results that can be obtained with this analysis.

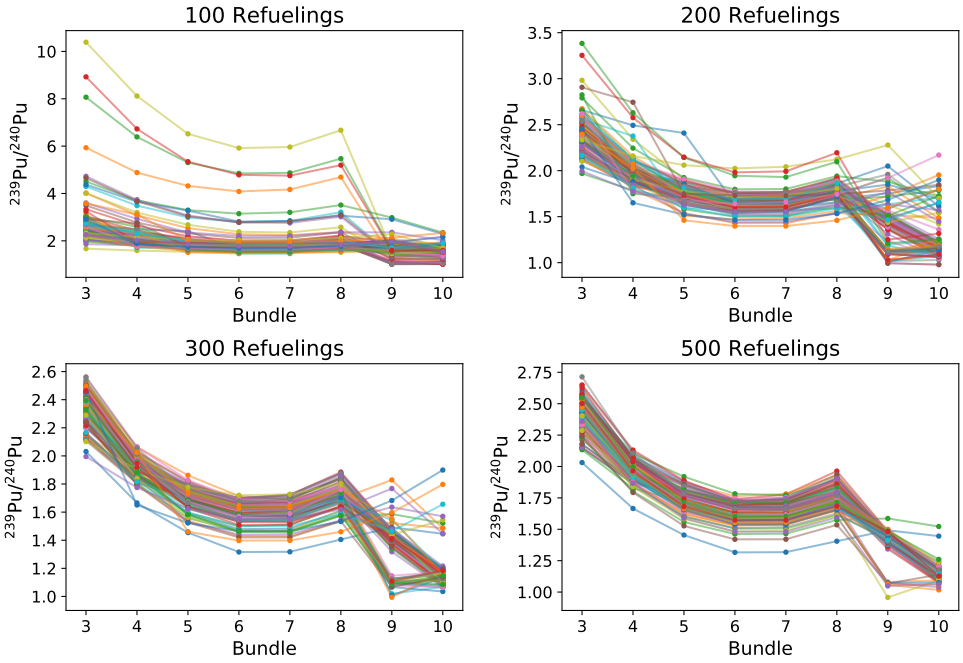

Figure 3.7. ^{239}Pu/^{240}Pu **ratios in each spent fuel bundle after 100, 200, 300, and 500 channel refuelings. The orientation of the data was realigned to show the previous channel refueling going from left to right for convergence analysis.**

Table 3.5. List of selected isotopes for detailed analysis.

Fission Products	Non-fission Products
^{131m}Xe	^{238}Pu
^{133m}Xe	^{239}Pu
^{133}Xe	^{240}Pu
^{134}Xe	^{241}Pu
^{135}Xe	^{234}U
^{136}Xe	^{235}U
^{133}Cs	^{236}U
^{135}Cs	^{238}U

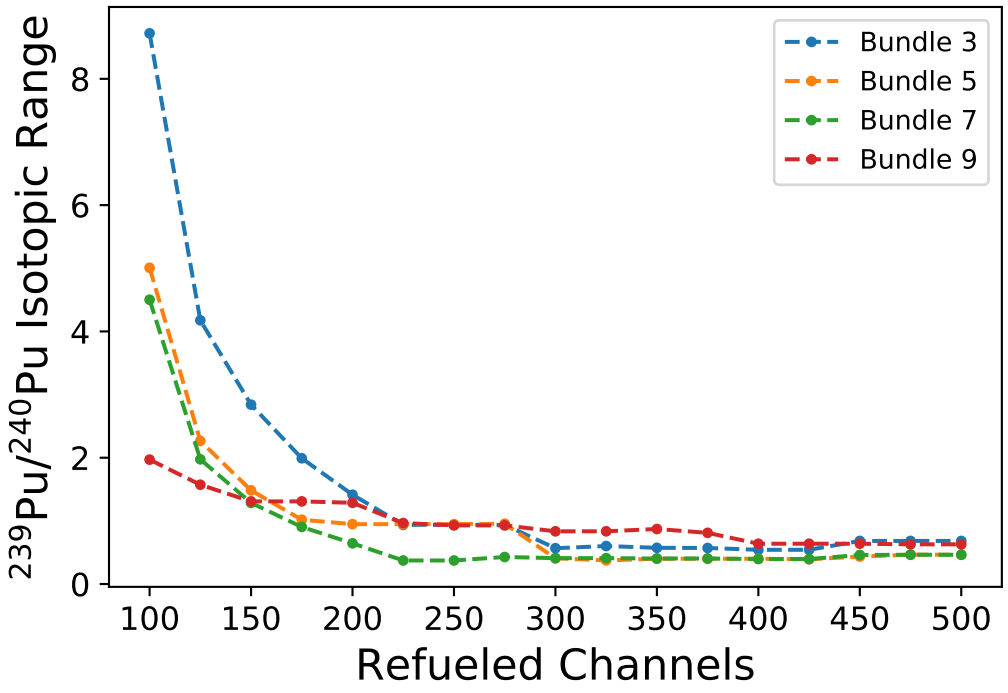

Figure 3.8. ^{239}Pu/^{240}Pu ranges in bundles 3, 5, 7, and 9 for each channel using increments of 25 refuelings.

IV. Results

The results of the quarter-core CANDU-6 model follow the outline laid out in Chapter 3. First, the flux profile and criticality results from the initial criticality model are discussed. Then, the spent fuel results of the burnup model are presented with examples to highlight the variation in isotopic concentration and isotope ratios that are present throughout the core. Finally, the initial criticality model is compared with the converged model after performing 500 refuelings.

4.1 Criticality Model

In Chapter 3, the quarter-core CANDU-6 criticality model was developed as the starting model for the burnup model and isotope production analysis. This model skips the initial startup process and provides an idealized, critical, steady-state model using an artificial burn of eight initial fuel bundle building blocks. From this model an insight in to the potential variations in the final results was obtained. The model simulated 2,250 generations of 200,000 neutrons and obtained an effective multiplication factor of $1.002440 \pm 2.2 \times 10^{-5}$. This indicates that it is a sufficient starting point of the burnup model to be able to maintain system criticality without modifying adjuster rod positions. An effective multiplication factor far from 1 would indicate an error in the geometry or material definitions.

Fission heat deposition detectors calculated the channel integrated power distribution of the quarter-core model as shown in Figure 4.1. The modeled distribution shows steep gradients in adjacent channel powers. This is due to the approximated initial bundle burnup profiles. The individual channel power ranges from 2.08 MW to 7.77 MW. For typical steady state operation of a CANDU-6 reactor, the distribution should average around 6.6 MW in the center channels and 3.0 MW in the outer ring

with a smooth gradient from the center of the core to the periphery with exceptions for small variations near recently refueled channels [16]. The power distribution in Figure 4.1 shows strong pockets of uneven burnup, especially around channels GA and EC compared to their symmetrical counterparts. In Section 4.3, the smoothing of this distribution from a set of channel burnups after 500 refuelings that is more representative of steady-state operations is discussed.

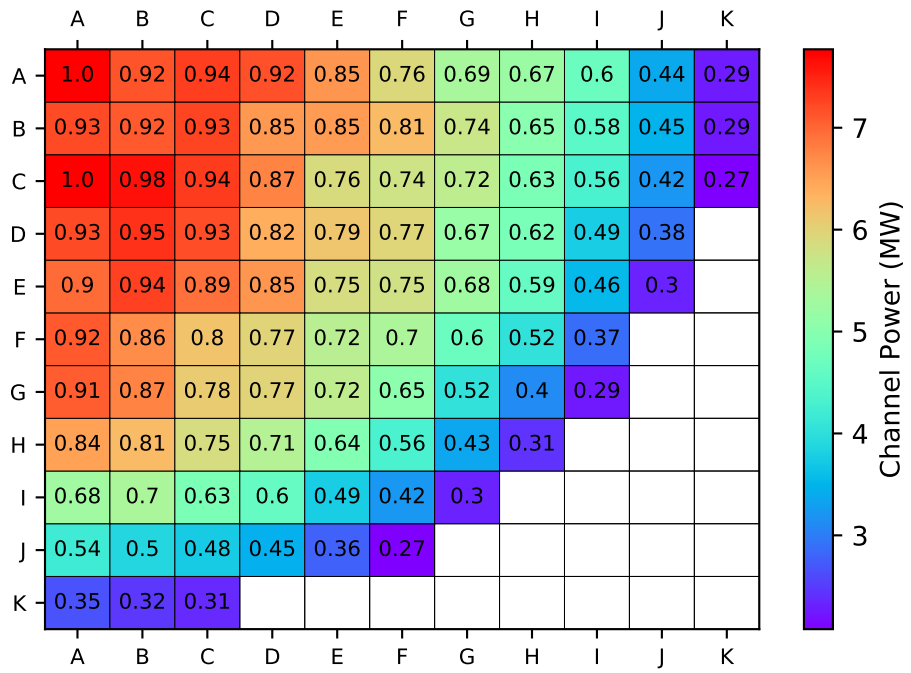

Figure 4.1. The channel integrated power distribution for the initial quarter-core CANDU-6 model. The axes correspond to the channel identification indexes used. Overlay values correspond to the channel power normalized to the hottest channel.

Two of the most bounding channels, AA and KA, were selected for spectrum analysis. A center bundle in channel AA, AA7, and an edge bundle in KA, KA1, were selected to show the normalized discrete energy spectrum differences in Figure 4.2. The difference in total flux between the two bundles was $46.1 \pm 4.6\%$. The normalized spectra show a strong difference of 30% around 1 eV. This is likely due to the neutron absorption in the adjuster rod near bundle AA7. Numerous differences that generally

fall in the 1-8% range fill the remainder of the spectrum. The differences in the epithermal region are of particular influence as they have a strong effect on the neutron capture rate for isotope production.

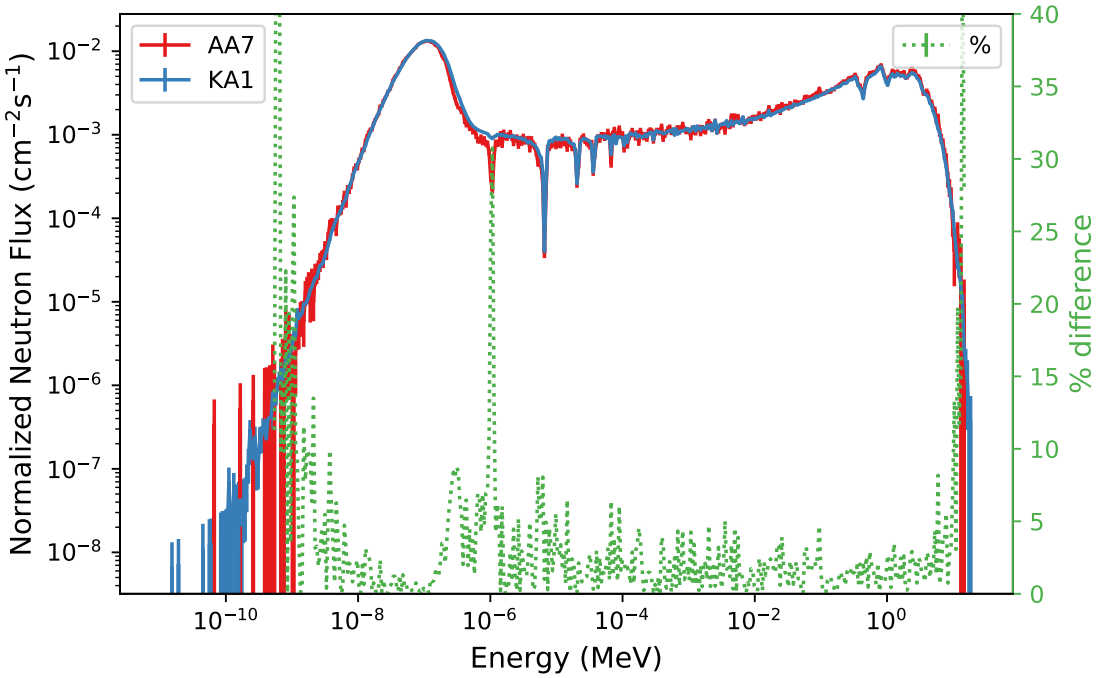

Figure 4.2. Comparison of the initial normalized neutron flux spectra between the center fuel bundle, AA7, and peripheral fuel bundle, KA1. The green dotted lines show the relative difference with the right y-axis.

4.2 Burnup Model

The quarter-core CANDU-6 criticality model was burned for 500 refuelings. This is equivalent to 1400 EFPD or 3.84 years of operation at full power. The large number of refuelings allowed the flux and burnup distributions to converge as shown in Sections 3.2.3. The eight spent fuel bundles from the most recent refueling for each channel was used to build a spent fuel isotopic concentration database consisting of 257 isotopic concentrations from 760 fuel bundles. All isotopic concentrations re-

ported, and derivative values such as isotopic ratios, are the concentration at removal from the reactor and have not been decayed post-irradiation.

Figure 4.3 shows an example isotopic ratio distribution, $^{239}Pu/^{240}Pu$, from the database. This distribution clearly demonstrates that the isotopic ratios are affected by their spatial location inside the reactor. The grouping of bundles around a ratio of 1.00-1.25 correspond to the two edge fuel bundles in each channel that saw three channel refuelings. These bundles burned for three channel refuelings because of the implementation of the swing-eight refueling-scheme. For example, bundles 1 and 2 remained stationary after the first burn where 11 and 12 were pushed through after removing the center 8 bundles. After the second burn, 1 and 2 were pushed through to now occupy positions 9 and 10. They were then removed after the third burn as part of the center 8 bundles. The remainder of the counts are from bundles that saw only one cycle in the reactor, but their ratios still vary significantly due to their axial position in the channel and the channel's radial position in the reactor.

Four additional actinide isotope ratios are displayed in Figure 4.4. These examples highlight the importance of the energy spectrum on radioisotopes produced through neutron activation, especially (n,γ) and (n,2n) reactions. The unique production cross section for each of the isotopes results in a wide range of possible actinide ratios based on the irradiation history for each bundle.

Four fission-product isotope ratios are also provided in Figure 4.5. All of these isotopes are, or start out as, fission-products. Fission product production is directly correlated to the power distribution. As shown in Figure 4.2, the majority of the flux is below 1 MeV, and the differences in the spectra are generally small in this region. Therefore, the fission product concentrations and resulting ratios are heavily dependent on their spatial fission rate and differences due to higher energy neutrons are small in comparison. The xenon isotopes, particularly ^{135}Xe, are fission-product

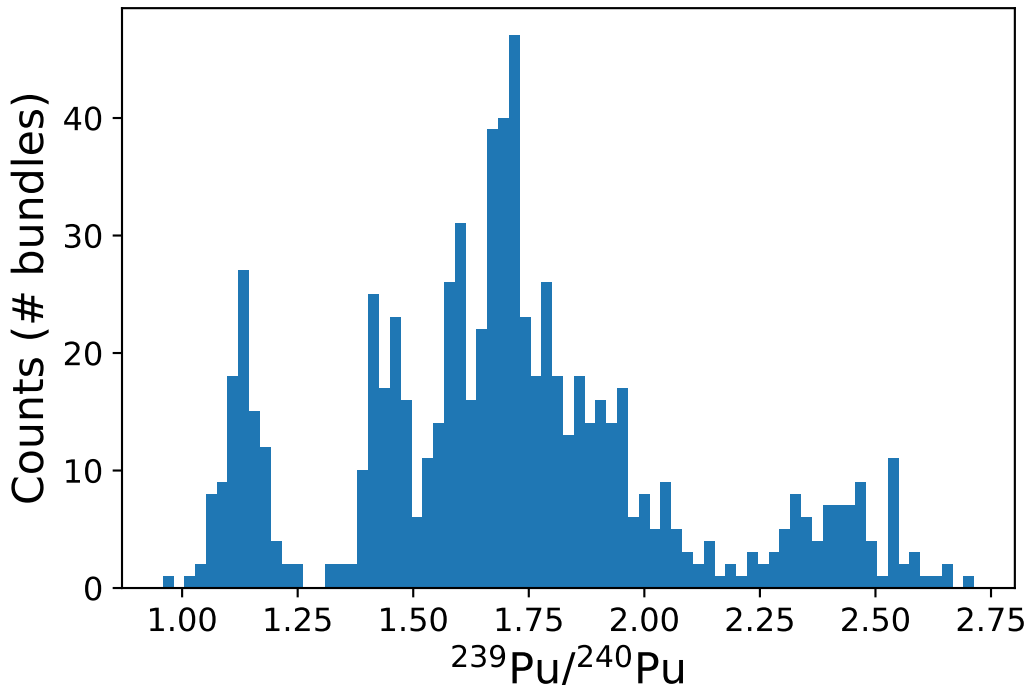

Figure 4.3. Distribution of isotopic ratios for ^{239}Pu/^{240}Pu from the 760 spent fuel bundles.

poisons, therefore, they generally follow the power distribution of the reactor.

The 1-D histogram distributions of the isotopic ratios do not convey the entire story. Many concentrations exhibit non-linear properties when tied together to form ratios. This adds an additional layer of complexity to the potential range of isotopic ratios from spent fuel. Figure 4.6 shows four actinide ratios in a 2-D histogram. The majority show curvature demonstrating a non-linear dependence of the spatial variance in production and loss.

The complexity of each of these distributions, combined with their dissimilarity to one another, makes standard statistical analysis difficult. The range and average of each distribution is easily determined, but quantifying their standard deviation is not as they do not follow standard distributions. To calculate a confidence interval (CI) to assist with assessments, bootstrapping was applied. 20,000 samples, with

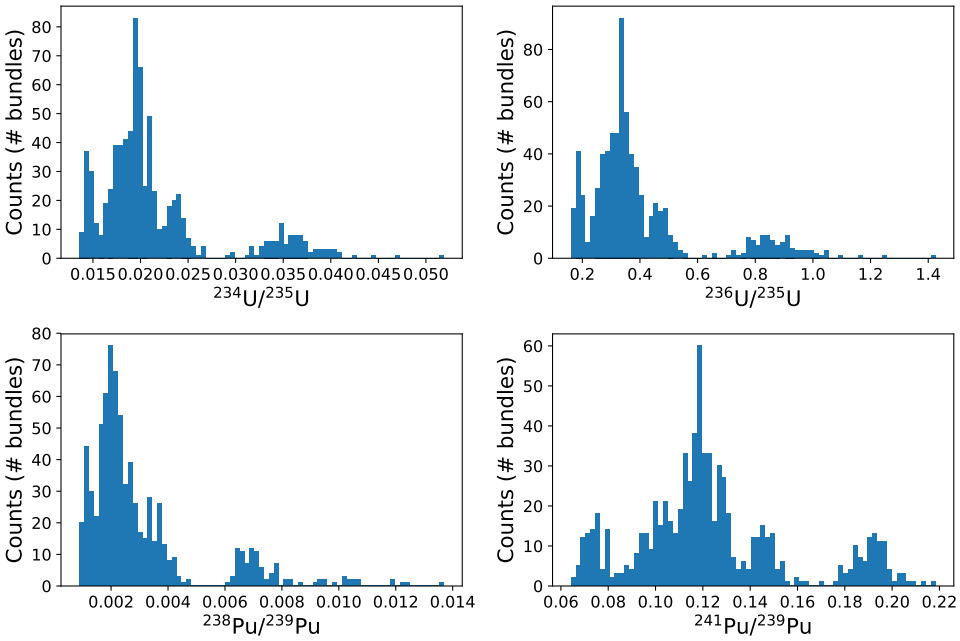

Figure 4.4. Isotopic ratio distributions for select actinides.

replacement, were drawn from each distribution to obtain a large sampling estimate and were used to calculate the 67%, 95%, and 99% confidence intervals. These values are listed in Table 4.1 along with the range and average for each of the selected ratios.

The ratios for $^{135}Xe/^{133}Xe$ and $^{133m}Xe/^{131m}Xe$ from the spent fuel database were included in the CTBTO xenon plot from Section 2.1 to highlight how the model results compare to measurements from various NPPs and MIPFs. Figure 4.7 shows the model predicted range in measurements from a CANDU-6 reactor results in a non-weapon source attribution for this particular signature. $^{135}Xe/^{133}Xe$ shows a range one order in magnitude while $^{133m}Xe/^{131m}Xe$ shows very little variation. It is important to note that this is the initial isotopic ratio seen post-refueling. Due to the range of half-lives (9.14 hours to 11.84 days), if the time of removal is not known precisely, the range covered would vary. While this particular signature is easily determined to be a non-weapons related release, this example illustrates the

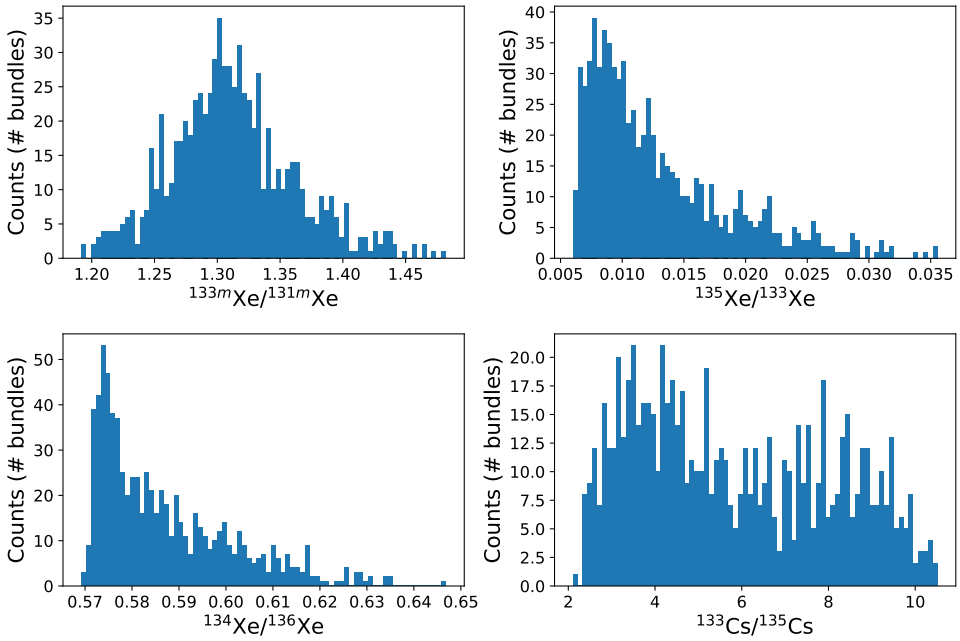

Figure 4.5. Isotopic ratio distributions for select fission-products. The groupings of bundles correspond to groupings observable in Figure 3.8; however, their exact origins are dependent on the isotopes in question.

Table 4.1. Statistics for select isotopic ratio distributions.

	Min	Max	Avg	67% CI	95% CI	99% CI
$\frac{^{234}\mathrm{U}}{^{235}\mathrm{U}}$	0.014	0.052	0.021	0.017 - 0.025	0.014 - 0.038	0.014 - 0.042
$\frac{^{236}\mathrm{U}}{^{235}\mathrm{U}}$	0.16	1.43	0.40	0.26 - 0.49	0.18 - 0.94	0.17 - 1.10
$\frac{^{239}\mathrm{Pu}}{^{238}\mathrm{Pu}}$	73.0	1134.9	450.3	257.4 - 622.4	107.7 - 953.0	83.7 - 1055.1
$\frac{^{239}\mathrm{Pu}}{^{240}\mathrm{Pu}}$	0.958	2.714	1.710	1.409 - 1.980	1.087 - 2.530	1.049 - 2.599
$\frac{^{241}\mathrm{Pu}}{^{239}\mathrm{Pu}}$	0.064	0.218	0.124	0.096 - 0.149	0.070 - 0.197	0.067 - 0.206
$\frac{^{133m}\mathrm{Xe}}{^{131m}\mathrm{Xe}}$	1.192	1.482	1.312	1.266 - 1.361	1.218 - 1.430	1.203 - 1.463
$\frac{^{135}\mathrm{Xe}}{^{133}\mathrm{Xe}}$	0.006	0.036	0.013	0.008 - 0.019	0.007 - 0.028	0.006 - 0.032
$\frac{^{134}\mathrm{Xe}}{^{136}\mathrm{Xe}}$	0.569	0.647	0.587	0.574 - 0.601	0.571 - 0.621	0.570 - 0.634
$\frac{^{133}\mathrm{Cs}}{^{135}\mathrm{Cs}}$	2.103	10.516	5.812	3.481 - 8.435	2.56 - 9.862	2.375 - 10.342

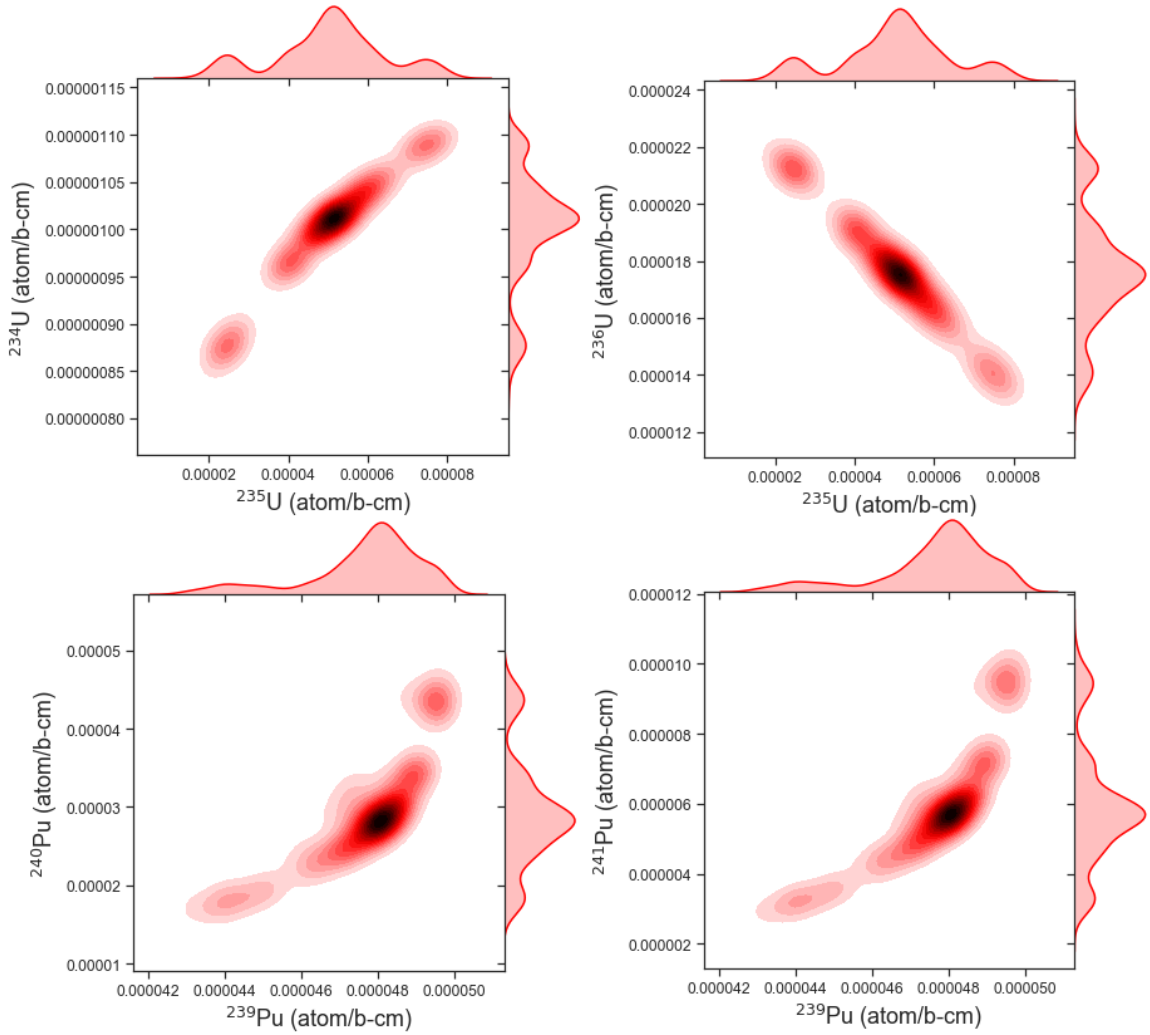

Figure 4.6. Heatmaps depicting the non-linearity of four actinide ratios.

utility of the analysis and the kind of information that can be obtained.

4.3 Steady State Criticality Model

After the conclusion of the 500^{th} refueling, a duplicate criticality calculation was performed. This provided results to compare to the initial model after the isotopic concentration and flux distributions were permitted to converge from burnup and refueling. The effective multiplication factor of the final model was $0.99811 \pm 2.3 \times 10^{-5}$ indicating the model maintained criticality well within the range of the adjuster rod

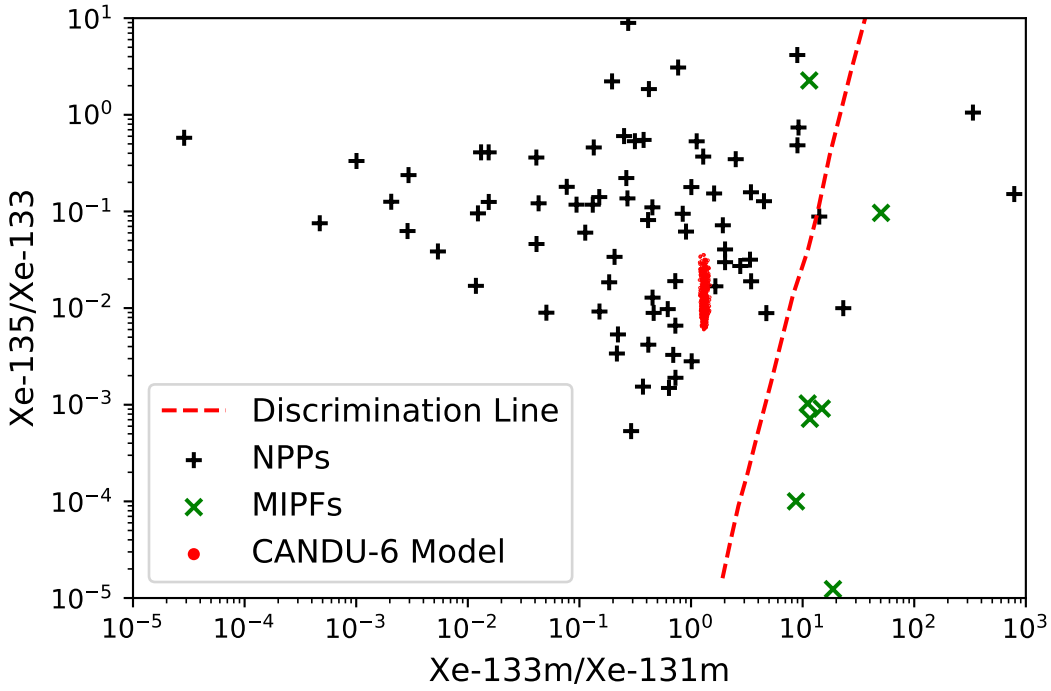

Figure 4.7. Xenon ratio results compared to CTBTO measurements [9]. This provides an application example as to how much a single signature might vary.

worth.

The normalized flux spectra plot for the final model, Figure 4.8, shares strong similarities with the initial model, Figure 4.2. The 30% difference at 1 eV remains; however, the upper edge of the thermal peak increased to 12% from 8%. The entire resonance region also has increased differences averaging around 3-6% from 1-3% in the initial model. The overall flux magnitude difference, $45.1 \pm 4.5\%$, is consistent with the initial model.

The biggest differences between the initial model and the final model are in the power distributions. Figure 4.9 shows the channel integrated power distributions for the initial and final models, respectively. The values in each channel indicate the channel power normalized to the hottest channel in the initial model. From the initial compared to the final, it is clear that channel-to-channel gradients have been reduced

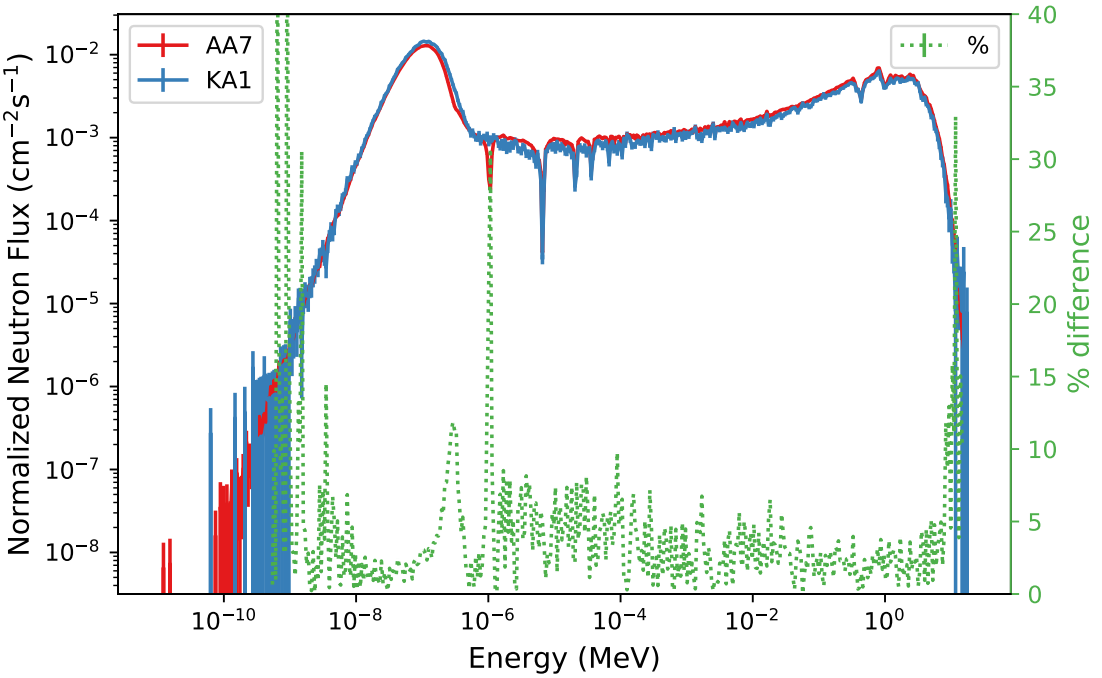

Figure 4.8. Comparison of the final normalized neutron flux spectra between the center fuel bundle, AA7, and peripheral fuel bundle, KA1. The green dotted lines show the relative difference with the right y-axis.

significantly. This is perhaps best illustrated in the comparison of the channel powers for GA and EC. The final power distribution obtained is more consistent with the expected distribution for steady-state operation of a CANDU-6 reactor compared to the initial distribution.

4.4 Edge Case Bundles

It was observed in Figure 4.3 that several spent fuel bundles showed ^{239}Pu/^{240}Pu ratios very close to 1. This indicated that there were points in the reactor that produced ^{240}Pu at a similar or faster rate than ^{239}Pu. These fuel bundles were identified as the "edge-case" bundles. Specifically, they are bundles 1, 2, 11, and 12 represented in Figure 2.10 for each channel. Further analysis was performed to better understand

the conditions that were causing these results.

Figure 4.10 shows the history of bundle positions BA11 and BA3 over the 500 total channel refuelings. The fuel bundle of interest is the one that starts fresh in position BA11 and moves to position BA3 after approximately 110 total refuelings, 300 EFPD, each time. This bundle then spends another 50 total refuelings, 140 EFPD, in position BA3 before it is removed and sent to spent fuel storage. The point of interest for this bundle is after it switches to position BA3. The concentration of ^{240}Pu continues to rise; however, the concentration of ^{239}Pu becomes constant. This is likely due to an equilibrium between the production and loss of ^{239}Pu at high burnup being achieved. The shift in neutron environment along with high burnup appears to allow ^{240}Pu to continue to rise while limiting the additional production of ^{239}Pu. This phenomena is present in every edge-case bundle in every channel.

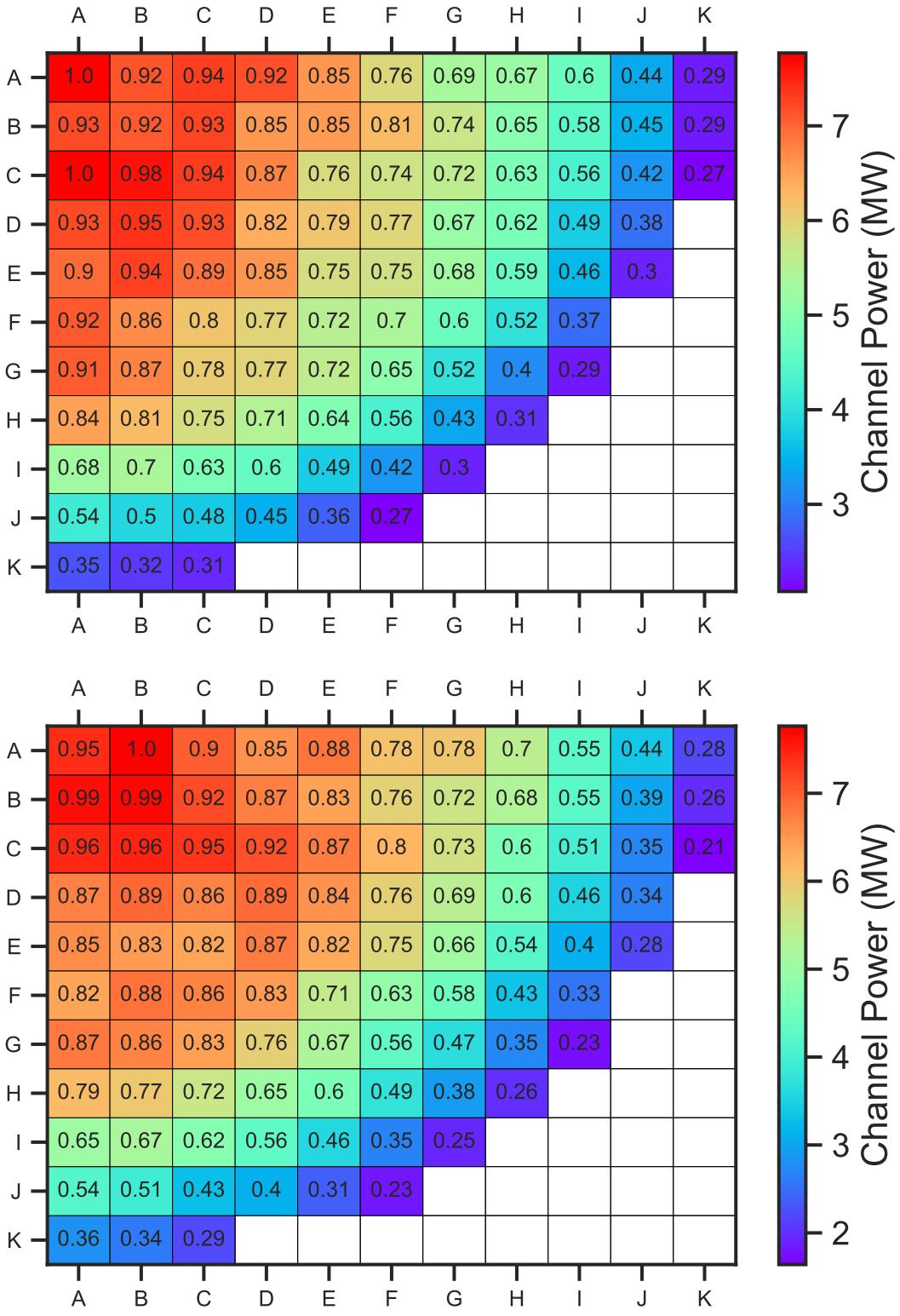

Figure 4.9. Channel integrated power distribution for the initial (top) and final (bottom) criticality models. The overlay values are the channel powers normalized to the peak channel power of the initial model.

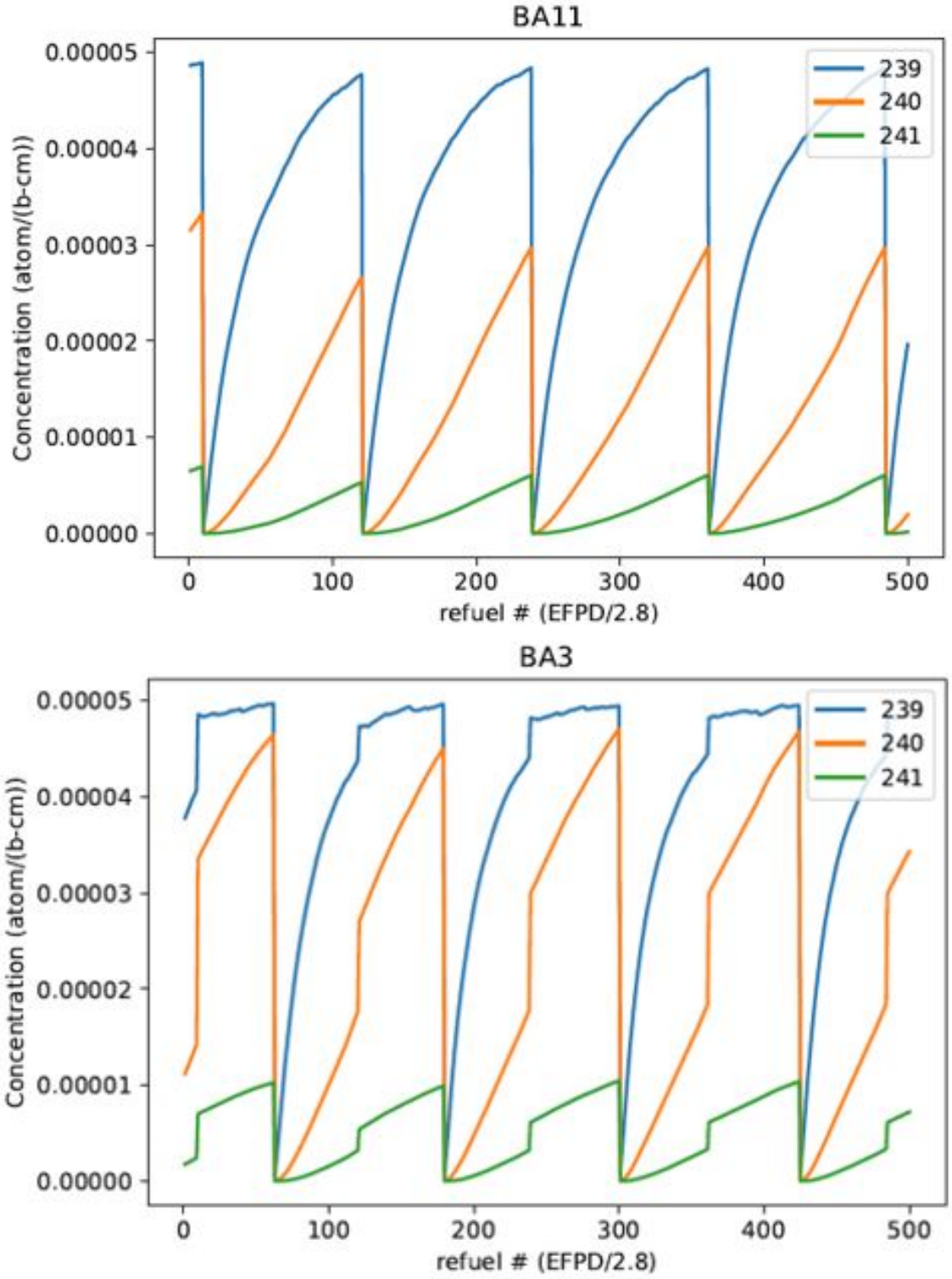

Figure 4.10. Plutonium analysis of one of four edge-case bundles in fuel channel BA. The observed fuel bundle starts in position BA11 and moves to position BA3.

V. Conclusion

The quarter-core CANDU-6 model provided the full isotopic concentration distribution of CANDU-6 spent fuel from standard operations. Previous efforts to characterize reactor signatures use approximations to obtain assembly level averaged values. This work modeled a quarter-core CANDU-6 reactor to mimic steady-state operations and obtain spatial distributions for isotopic concentrations and ratios.

To develop the isotopic concentration database, a generic CANDU-6 reactor was modeled in Serpent 2. An initial model was built using artificially burned fuel bundles to create a steady-state critical model for fuel depletion and refueling. This model showed a relative flux magnitude difference of $46.1 \pm 4.6\%$ across the core with with discrete energy differences ranging from 1-30%

The model was then burned for 500 channel refueling cycles, 1400 EFPD, to converge the spatial flux and burnup distributions and obtain spent fuel isotopic concentrations. An isotopic concentration database contains the expected distributions for 257 isotopes from 760 spatial locations within the CANDU-6 core which can be used as a tool for treaty monitoring and future research. Analyzed isotopic concentrations and ratios displayed complex and unique distributions that made analytic modeling difficult to impossible.

Select fission product and actinide isotopic ratio distributions were analysed in detail to highlight the information extractable from these models. These contain not only the most probable values and potential ranges but complete probabilities for each concentration. For each of the nine actinide and fission product ratios, the mean, range, and 67%, 95%, and 99% confidence intervals were quantified. The confidence intervals were quantified using bootstrapping with replacement to measure to the complex, and varied, distributions for each of the isotopic ratios considered. Finally, an example comparison was made with Xenon ratios to CTBTO reported

measurements that demonstrated noticeable variance for these signatures.

These expected isotopic ratio distributions provide the needed resolution of potential variance missing in previous spatially averaged analyses. Averaged isotopic ratio values from the database provide the most probable expected measurements; however, this analysis supplements and extends those analyses to include the full plausible range to help analyze ambiguous signatures. In this sense, this research sets the framework for future source term analysis for nuclear treaty monitoring that can reduce false positive rates.

5.1 Future Research

The quarter-core CANDU-6 spatial spent fuel analysis provided possible isotopic concentration results for a single reactor design operating under standard procedures. This provides the expected range of signatures for a CANDU-6 for the International Monitoring System; however, there are numerous reactor designs and countless operational possibilities for each that are worth considering. To further this research, there are two avenues that are recommended for further exploration:

- The first avenue is a direct reproduction of this work for other reactor designs. This can expand the spent fuel isotope database to include the expected isotopic concentrations for all reactors of interest. Each additional design can potentially help increase resolution for non-proliferant activities and clearly identify areas of ambiguity.

- The second avenue is to reevaluate spatial models assuming non-standard procedures such as transients, startup, and alternate burnup profiles. This could provide increased understanding of the range of signatures that can be expected at IMS stations.

Appendix A. Initial Fuel Loading Pattern

Table A.1. Fuel burnups used in the initial fuel loading pattern. The index corresponds to the fuel bundles in Table 3.3 and Appendix A [7].

Index	Burnup (MWd/MTU)
1	32.69
2	78.38
3	342.37
4	818.87
5	1638.73
6	3608.15
7	6381.44
8	8721.49

Table A.2. CANDU-6 axial layer 1 initial burnup fuel loading pattern [7].

	A	B	C	D	E	F	G	H	I	J	K
A	7	5	8	3	7	5	8	4	7	4	7
B	5	8	4	8	4	7	4	5	4	7	3
C	7	3	7	5	8	5	7	5	8	1	8
D	5	8	2	8	5	7	5	7	5	7	
E	8	3	7	3	8	4	7	3	7	4	
F	5	8	5	7	5	7	4	7	4		
G	7	4	8	4	6	3	7	4	7		
H	1	7	1	7	4	7	4	8			
I	7	3	7	3	8	2	7				
J	3	7	4	7	3	7					
K	7	4	7								

Table A.3. CANDU-6 axial layer 2 initial burnup fuel loading pattern [7].

	A	B	C	D	E	F	G	H	I	J	K
A	7	6	8	3	8	6	8	6	7	6	7
B	6	8	6	8	5	7	5	6	5	7	5
C	7	4	7	6	8	6	7	6	7	1	7
D	6	8	3	8	6	7	6	7	6	7	
E	8	5	8	4	8	5	7	4	7	6	
F	6	8	6	8	6	7	6	7	6		
G	7	5	8	5	7	4	7	6	6		
H	2	7	1	7	5	7	5	7			
I	8	4	7	3	8	3	7				
J	5	7	5	7	5	7					
K	7	6	7								

Table A.4. CANDU-6 axial layer 3 initial burnup fuel loading pattern [7].

	A	B	C	D	E	F	G	H	I	J	K
A	7	6	7	4	8	6	8	6	6	6	7
B	7	8	6	8	5	6	5	7	6	7	6
C	7	5	7	6	8	6	7	6	7	1	6
D	7	8	3	8	6	7	6	7	6	7	
E	8	5	7	4	8	5	6	4	6	6	
F	6	8	7	8	7	7	6	6	6		
G	7	6	8	6	7	4	7	6	6		
H	2	7	1	7	6	7	6	7			
I	7	4	7	4	8	3	7				
J	5	7	6	6	5	6					
K	7	6	7								

Table A.5. CANDU-6 axial layer 4 initial burnup fuel loading pattern [7].

	A	B	C	D	E	F	G	H	I	J	K
A	6	7	7	4	7	7	8	6	6	7	7
B	7	7	6	8	6	6	6	7	6	6	6
C	6	5	6	6	8	7	6	7	6	1	5
D	7	7	3	8	6	6	7	6	7	6	
E	7	5	7	4	7	5	5	5	6	7	
F	6	7	7	7	7	6	6	6	6		
G	6	6	7	6	6	5	7	6	5		
H	3	7	2	6	6	6	6	7			
I	7	5	7	4	7	3	7				
J	6	7	6	6	6	6					
K	7	7	6								

Table A.6. CANDU-6 axial layer 5 initial burnup fuel loading pattern [7].

	A	B	C	D	E	F	G	H	I	J	K
A	4	7	6	4	6	7	7	6	5	7	7
B	7	7	6	7	6	4	6	7	6	6	6
C	5	5	6	6	8	7	6	7	5	1	3
D	7	6	3	7	6	6	7	6	7	6	
E	7	5	6	5	7	6	4	5	6	7	
F	6	7	7	7	7	6	6	5	7		
G	6	6	7	6	5	5	7	7	4		
H	3	6	2	6	6	5	6	6			
I	7	5	7	5	7	4	7				
J	6	7	6	5	6	6					
K	6	7	6								

Table A.7. CANDU-6 axial layer 6 initial burnup fuel loading pattern [7].

	A	B	C	D	E	F	G	H	I	J	K
A	4	7	6	4	6	7	7	6	5	7	7
B	7	7	6	7	6	4	6	7	6	6	6
C	5	5	6	6	8	7	6	7	5	2	3
D	7	6	3	7	7	6	7	6	7	6	
E	7	5	6	5	7	6	4	5	6	7	
F	6	7	8	7	7	6	7	5	7		
G	6	6	7	6	4	5	7	7	4		
H	3	6	2	6	6	5	6	6			
I	7	5	7	5	7	4	7				
J	6	7	6	5	6	6					
K	7	7	6								

Table A.8. CANDU-6 axial layer 7 initial burnup fuel loading pattern [7].

	A	B	C	D	E	F	G	H	I	J	K
A	4	7	6	4	6	7	7	6	5	7	7
B	7	7	6	7	6	4	6	7	6	6	6
C	5	5	6	6	8	7	6	7	5	2	3
D	7	6	3	7	7	6	7	6	7	6	
E	7	5	6	5	7	6	4	5	6	7	
F	6	7	8	7	7	6	7	5	7		
G	6	6	7	6	4	5	7	7	4		
H	3	6	2	6	6	5	6	6			
I	7	5	7	5	7	4	7				
J	6	7	6	5	6	6					
K	7	7	6								

Table A.9. CANDU-6 axial layer 8 initial burnup fuel loading pattern [7].

	A	B	C	D	E	F	G	H	I	J	K
A	4	7	6	4	6	7	7	6	5	7	6
B	7	7	6	7	6	4	6	7	6	6	6
C	5	5	6	6	8	7	6	7	5	1	3
D	7	6	3	7	6	5	7	6	7	6	
E	7	5	6	5	7	6	4	5	6	7	
F	6	7	7	7	7	6	6	5	7		
G	6	6	7	6	4	5	7	7	3		
H	3	6	2	6	6	5	6	6			
I	7	5	7	5	7	4	7				
J	6	7	6	5	6	6					
K	6	7	6								

Table A.10. CANDU-6 axial layer 9 initial burnup fuel loading pattern [7].

	A	B	C	D	E	F	G	H	I	J	K
A	4	7	6	6	6	7	7	7	5	7	6
B	8	7	7	7	6	4	6	7	6	6	6
C	5	6	6	7	8	7	6	7	4	5	3
D	7	6	6	7	7	5	7	6	7	6	
E	7	6	6	6	7	6	4	6	5	7	
F	7	6	8	7	7	6	7	5	7		
G	5	6	7	6	4	6	6	7	3		
H	5	6	5	6	6	5	6	6			
I	6	6	6	6	7	5	6				
J	6	6	6	5	6	5					
K	6	7	6								

Table A.11. CANDU-6 axial layer 10 initial burnup fuel loading pattern [7].

	A	B	C	D	E	F	G	H	I	J	K
A	4	8	6	7	6	8	7	7	5	7	6
B	8	7	7	7	7	4	7	7	7	6	7
C	4	7	6	8	7	8	6	7	4	6	3
D	7	6	6	7	7	5	8	6	8	6	
E	6	7	6	7	6	7	3	6	5	7	
F	7	6	8	6	8	6	7	5	7		
G	5	7	7	7	4	6	6	7	3		
H	6	6	6	6	7	5	7	6			
I	6	6	6	6	6	6	6				
J	6	6	7	5	6	5					
K	6	7	6								

Table A.12. CANDU-6 axial layer 11 initial burnup fuel loading pattern [7].

	A	B	C	D	E	F	G	H	I	J	K
A	3	8	5	7	6	8	6	8	4	8	5
B	8	6	7	6	8	3	7	6	7	5	7
C	4	8	5	8	6	8	5	7	3	7	3
D	6	5	7	6	8	5	8	5	8	5	
E	6	8	6	7	6	7	3	7	5	7	
F	8	6	8	6	8	5	7	4	7		
G	5	7	6	7	3	7	6	7	3		
H	6	5	7	5	7	4	7	5			
I	6	7	6	7	6	7	5				
J	7	6	7	4	7	4					
K	5	7	5								

Table A.13. CANDU-6 axial layer 12 initial burnup fuel loading pattern [7].

	A	B	C	D	E	F	G	H	I	J	K
A	3	8	4	7	5	8	5	8	3	8	4
B	8	5	7	5	8	3	7	5	7	4	7
C	3	8	4	8	5	8	4	7	3	7	2
D	5	4	7	5	7	3	7	4	8	4	
E	5	8	5	8	5	7	3	7	3	7	
F	7	5	8	5	8	4	7	3	8		
G	3	7	5	7	3	7	4	7	2		
H	7	4	7	4	7	3	7	4			
I	4	7	4	7	5	7	4				
J	7	4	7	3	7	3					
K	4	7	4								

Appendix B. Github Repository

The input files and post-processing scripts used in this research are available online via the AFIT WING GitHub Organization. These serve as documentation for reproducibility and reference for future work. The types of files available are scripts used for creating input files, model input files, automation scripts, and post-processing scripts. All scripts use Python 3 and the SerpentTools packages available here.
The model input files are written for Serpent 2. The CANDU-6 spent fuel isotopic concentration database is also available in the repository.

The main repository consists of the thesis, a README detailing the structure of the repository, and sub-folders for each model and results. The sub-folders are as follows:

- Bundleburn:

The Bundleburn folder contains the input files used to perform the artificial bundle burn for the criticality model.

- Critmodel:

The Critmodel folder contains the Python 3 scripts used for building the initial quarter-core model, the model input files for Serpent 2, and the results of the initial model.

- Burnmodel:

The Burnmodel folder contains the model input files for the depletion of the quarter-core model, the monitoring tools, the refueling and automation tools, and the results. The raw data obtained from the burnmodel is not available due to its size.

- Critmodel2:

The Critmodel folder contains the model input files for the final model after the 500^{th} refueling, and the results of the final model.

Appendix C. Tracked Isotopes

Table C.1. Isotopes available in the CANDU-6 spent fuel database.

^{109}Ag	^{140}Ce	^{154}Eu	^{113}In	^{147}Nd	^{241}Pu	^{82}Se	^{99}Tc	^{131m}Xe
^{110m}Ag	^{141}Ce	^{155}Eu	^{115}In	^{148}Nd	^{242}Pu	^{147}Sm	^{122}Te	^{132}Xe
^{111}Ag	^{142}Ce	^{156}Eu	^{80}Kr	^{150}Nd	^{243}Pu	^{148}Sm	^{123}Te	^{133}Xe
^{241}Am	^{143}Ce	^{157}Eu	^{82}Kr	^{236}Np	^{244}Pu	^{149}Sm	^{124}Te	^{133m}Xe
^{242}Am	^{144}Ce	^{69}Ga	^{83}Kr	^{237}Np	^{85}Rb	^{150}Sm	^{125}Te	^{134}Xe
^{242m}Am	^{242}Cm	^{71}Ga	^{84}Kr	^{238}Np	^{86}Rb	^{151}Sm	^{126}Te	^{135}Xe
^{243}Am	^{243}Cm	^{152}Gd	^{85}Kr	^{239}Np	^{87}Rb	^{152}Sm	^{127m}Te	^{136}Xe
^{244}Am	^{244}Cm	^{154}Gd	^{86}Kr	^{16}O	^{103}Rh	^{153}Sm	^{128}Te	^{89}Y
^{244m}Am	^{245}Cm	^{155}Gd	^{138}La	^{17}O	^{105}Rh	^{154}Sm	^{129m}Te	^{90}Y
^{75}As	^{246}Cm	^{156}Gd	^{139}La	^{231}Pa	^{100}Ru	^{115}Sn	^{130}Te	^{91}Y
^{134}Ba	^{133}Cs	^{157}Gd	^{140}La	^{104}Pd	^{101}Ru	^{116}Sn	^{132}Te	^{66}Zn
^{135}Ba	^{134}Cs	^{158}Gd	^{100}Mo	^{105}Pd	^{102}Ru	^{117}Sn	^{230}Th	^{67}Zn
^{136}Ba	^{135}Cs	^{160}Gd	^{94}Mo	^{106}Pd	^{103}Ru	^{118}Sn	^{232}Th	^{68}Zn
^{137}Ba	^{136}Cs	^{72}Ge	^{95}Mo	^{107}Pd	^{104}Ru	^{119}Sn	^{234}Th	^{70}Zn
^{138}Ba	^{137}Cs	^{73}Ge	^{96}Mo	^{108}Pd	^{105}Ru	^{120}Sn	^{169}Tm	^{90}Zr
^{140}Ba	^{160}Dy	^{74}Ge	^{97}Mo	^{110}Pd	^{106}Ru	^{122}Sn	^{233}U	^{91}Zr
^{79}Br	^{161}Dy	^{76}Ge	^{98}Mo	^{147}Pm	^{99}Ru	^{123}Sn	^{234}U	^{92}Zr
^{81}Br	^{162}Dy	^{1}H	^{99}Mo	^{148}Pm	^{121}Sb	^{124}Sn	^{235}U	^{93}Zr
^{108}Cd	^{163}Dy	^{2}H	^{15}N	^{148m}Pm	^{123}Sb	^{125}Sn	^{236}U	^{94}Zr
^{110}Cd	^{164}Dy	^{4}He	^{93}Nb	^{149}Pm	^{124}Sb	^{126}Sn	^{237}U	^{95}Zr
^{111}Cd	^{166}Er	^{165}Ho	^{94}Nb	^{151}Pm	^{125}Sb	^{86}Sr	^{238}U	^{96}Zr
^{112}Cd	^{167}Er	^{127}I	^{95}Nb	^{141}Pr	^{126}Sb	^{87}Sr	^{239}U	
^{113}Cd	^{168}Er	^{129}I	^{142}Nd	^{142}Pr	^{76}Se	^{88}Sr	^{240}U	
^{114}Cd	^{170}Er	^{130}I	^{143}Nd	^{143}Pr	^{77}Se	^{89}Sr	^{128}Xe	
^{115m}Cd	^{151}Eu	^{131}I	^{144}Nd	^{238}Pu	^{78}Se	^{90}Sr	^{129}Xe	
^{116}Cd	^{152}Eu	^{133}I	^{145}Nd	^{239}Pu	^{79}Se	^{159}Tb	^{130}Xe	
^{139}Ce	^{153}Eu	^{135}I	^{146}Nd	^{240}Pu	^{80}Se	^{160}Tb	^{131}Xe	

Bibliography

1. M. B. D. Nikitin, "Comprehensive nuclear-test-ban treaty: Background and current developments," Congressional Research Service, Tech. Rep. 7-5700, 2016.

2. "Annual report 2017," CTBTO Preparatory Commission, Tech. Rep. CTBT/ES/2017/5, 2017. [Online]. Available: https://www.ctbto.org/fileadmin/user_upload/pdf/Annual_Report_2017/English/00-CTBTO_AR_2017_EN.pdf

3. M. Robel and M. J. Kristo, "Discrimination of source reactor type by multivariate statistical analysis of uranium and plutonium isotopic concentrations in unknown irradiated nuclear fuel material," *Journal of Environmental Radioactivity*, vol. 99, no. 11, pp. 1789–1797, 2008. [Online]. Available: http://dx.doi.org/10.1016/j.jenvrad.2008.07.004

4. M. Robel, B. Isselhardt *et al.*, "A composite position independent monitor of reactor fuel irradiation using Pu, Cs, and Ba isotope ratios," *Journal of Environmental Radioactivity*, vol. 195, no. August, pp. 9–19, 2018.

5. M. Oktavian, A. Agung, and H. Andang, "Fuel loading pattern optimization with constraint on fuel assembly inventory using quantum-inspired evolutionary algorithm," *E3S Web of Conferences*, no. 42, 2018.

6. B. T. Rearden and M. A. Jessee, "Scale code system," Oak Ridge National Laboratory, Oak Ridge, TN, Tech. Rep. ORNL/TM-2005/39, 2018. [Online]. Available: https://www.ornl.gov/sites/default/files/SCALE_6.2.3.pdf

7. J. M. Pounders, F. Rahnema *et al.*, "A 3D stylized half-core CANDU benchmark problem," *Annals of Nuclear Energy*, vol. 38, no. 4, pp. 876–896, 2011. [Online]. Available: http://dx.doi.org/10.1016/j.anucene.2010.10.018

8. J. Leppänen, "The serpent monte carlo code: Status, development and applications in 2013." *Annals of Nuclear Energy*, vol. 82, pp. 142–150, 2015.

9. C. Gueibe, M. B. Kalinowski *et al.*, "Setting the baseline for estimated background observations at IMS systems of four radioxenon isotopes in 2014," *Journal of Environmental Radioactivity*, vol. 178-179, no. September, pp. 297–314, 2017.

10. H. W. L. M. Benedict, T. H. Pigford, *Nuclear Chemical Engineering*, 2nd ed. McGraw-Hill Education, 1981.

11. B. Reed, "Understanding plutonium production in nuclear reactors," *The Physics Teacher*, vol. 43, no. 4, pp. 222–224, 2005.

12. M. B. Chadwick, "ENDF/B-VII.1 Nuclear Data for Science and Technology: Cross Sections, Covariances, Fission Product Yields and Decay Data," *Nuclear Data Sheets*, vol. 112, pp. 2887–2996, 2011.

13. J. R. Lamarsh and A. J. Baratta, *Introduction to Nuclear Engineering.* Upper Saddle River, NJ: Prentice-Hall, Inc, 2001.

14. "Nuclear reactor types," Savoy Place: IET London, The Institution of Electrical Engineers, 2005. [Online]. Available: http://large.stanford.edu/courses/2013/ph241/kallman1/docs/nuclear_reactors.pdf

15. "Applications of research reactors," International Atomic Energy Agency, Tech. Rep. NP-T-5.3, 2014. [Online]. Available: https://www-pub.iaea.org/MTCD/Publications/PDF/Pub1627_web.pdf

16. B. Rouben, "Candu fuel-management course," Atomic Energy of Canada Ltd., 2002. [Online]. Available: https://canteach.candu.org/Content%20Library/20031101.pdf

17. J. Leppänen, "Performance of woodcock delta-tracking in lattice physics applications using the serpent monte carlo reactor physics burnup calculation code," *Annals of Nuclear Energy*, no. 37, pp. 715–722, 2010.

18. E. R. Woodcock, T. Murphy, P. J. Hemmings, and T. C. Longworth, "Techniques used in the gem code for monte carlo neutronics calculations in reactors and other systems of complex geometry." Argonne National Laboratory, Tech. Rep. ANL-7050, 1965.

19. J. Leppänen, "Two practical methods for unionized energy grid construction in continuous-energy Monte Carlo neutron transport calculation," *Annals of Nuclear Energy*, vol. 36, no. 7, pp. 878–885, 2009. [Online]. Available: http://dx.doi.org/10.1016/j.anucene.2009.03.019

20. T. Viitanen, "Implementing a doppler-preprocessor of cross section libraries in reactor physics code serpent." Master's thesis, Helsinki University of Technology, 2009.

21. A. E. Isotalo and P. A. Aarnio, "Higher order methods for burnup calculations with bateman solutions," *Annals of Nuclear Energy*, no. 38, pp. 1987–1995, 2011.

22. A. E. Isotalo, "Substep methods for burnup calculations with bateman solutions," *Annals of Nuclear Energy*, no. 38, pp. 2509–2514, 2011.

REPORT DOCUMENTATION PAGE

Form Approved
OMB No. 0704–0188

1. REPORT DATE *(DD–MM–YYYY)*	2. REPORT TYPE	3. DATES COVERED *(From — To)*
26–03–2020	Master's Thesis	Jun 2018 — Mar 2020

4. TITLE AND SUBTITLE

An Assessment of the Spatial Variation of Isotopic Ratios in a CANDU-6 Reactor for Nuclear Treaty Monitoring

5a. CONTRACT NUMBER

5b. GRANT NUMBER

5c. PROGRAM ELEMENT NUMBER

6. AUTHOR(S)

2d Lt Aaron W. Burkhardt

5d. PROJECT NUMBER

5e. TASK NUMBER

5f. WORK UNIT NUMBER

7. PERFORMING ORGANIZATION NAME(S) AND ADDRESS(ES)

Air Force Institute of Technology
Graduate School of Engineering Physics (AFIT/ENP)
2950 Hobson Way
WPAFB OH 45433-7765

8. PERFORMING ORGANIZATION REPORT NUMBER

AFIT-ENP-MS-20-M-086

9. SPONSORING / MONITORING AGENCY NAME(S) AND ADDRESS(ES)

Air Force Technical Applications Center
POC: MAJ Brett Castle (brett.castle@us.af.mil)
10989 S Patrick Dr
Patrick AFB, FL 32925

10. SPONSOR/MONITOR'S ACRONYM(S)

AFTAC

11. SPONSOR/MONITOR'S REPORT NUMBER(S)

12. DISTRIBUTION / AVAILABILITY STATEMENT

APPROVED FOR PUBLIC RELEASE; DISTRIBUTION UNLIMITED.

13. SUPPLEMENTARY NOTES

14. ABSTRACT

The Preparatory Commission for the Comprehensive Nuclear Test Ban Treaty Organization developed the International Monitoring System for monitoring for nuclear explosive testing and compliance with nuclear treaties. Many of the International Monitoring System stations are capable of detecting radionuclides that can be used to determine their origin and creation environment. However, there is not a single unique signature associated with each creation environment. Nuclear reactors, for example, can have a wide range of isotopic concentrations caused by spatial variations in neutron flux intensity and energy. As a single sample only provides a single isotopic measurement, this can make disambiguation difficult for systems that have varying, and potentially overlapping, signatures. To better quantify this phenomena, a 3-D quarter-core CANDU-6 was modeled using Serpent 2 to analyze the spatial flux distribution and develop a spent fuel isotopic database. The model showed an overall relative flux magnitude difference of $45.1 \pm 4.5\%$ and significant differences in discrete neutron energies ranging from 1 to 30%. The developed database provides the full spatial isotopic distribution for 257 isotopes expected from CANDU-6 spent fuel. Actinide and fission product isotopic ratios were analyzed to determine their range and associated confidence intervals. The ratios showed significant bundle-to-bundle variance and significant inter-isotopic distribution variance making it difficult to accurately assess the range of possibilities from analytic methods. The developed CANDU-6 spatial isotopic database provides the increased resolution for future analysis of International Monitoring System signatures thereby enhancing the capabilities of the system to effectively perform their treaty monitoring mission.

15. SUBJECT TERMS

CANDU, Isotopic Variance, Monte-Carlo Transport, Non-Proliferation, Nuclear Forensics

16. SECURITY CLASSIFICATION OF:			17. LIMITATION OF ABSTRACT	18. NUMBER OF PAGES	19a. NAME OF RESPONSIBLE PERSON
a. REPORT	b. ABSTRACT	c. THIS PAGE			Maj James E. Bevins, AFIT/ENP
U	U	U	U	82	19b. TELEPHONE NUMBER *(include area code)* (937) 255-3636, x4767; james.bevins@afit.edu